

# 四川盆地西南缘龙马溪组泥岩地球化学特征及物源区和构造背景分析

张茜<sup>1,2,3)</sup>,肖渊甫<sup>1)</sup>,王晓飞<sup>2,3)</sup>,余谦<sup>2,3)</sup>,王剑<sup>4)</sup>,赵安坤<sup>1,2,3)</sup>,门玉澎<sup>2,3)</sup>,周业鑫<sup>2,3)</sup>

1)成都理工大学地球科学学院,成都,610059;

2)中国地质调查局成都地质调查中心,成都,610081;

3)自然资源部沉积盆地与油气资源重点实验室,成都,610081;

4)西南石油大学地球科学与技术学院,成都,610500

**内容提要:**本文对川西南荣经地区龙马溪组泥岩的岩石学、矿物学及元素地球化学开展了研究,探讨了龙马溪组沉积环境、物源区属性及构造背景。结果表明,研究区龙马溪组泥岩砂质、钙质含量较高,指示其沉积水体较浅。稀土元素特征及及 A—CN—K 图解说明龙马溪组泥岩组成较少受成岩及交代作用影响,样品较完整地保存了物源和风化作用信息。 $K_2O$ 、 $Rb$ 、 $Al_2O_3/TiO_2$  含量较高及 Eu 负异常指示其母岩为偏酸性的长英质岩、花岗岩类,推测主要来自康滇古陆新元古代早期地台盖层。 $ICV$  值大于 1,  $CIA$  平均值为 66,  $Th/U$  与地壳 UCC 值相近,  $Rb/Sr$  值明显低于 PAAS,指示其物源为近源初次旋回的快速沉积产物,受化学风化作用较小,沉积环境为干燥、寒冷环境。 $La/Yb$ 、 $LREE/HREE$  及  $Sc/Cr$  等值均与被动大陆边缘值相近,结合  $Sc/Cr-La/Y$  等判别图解,说明研究区沉积构造背景主要为被动大陆边缘。

**关键词:**龙马溪组;地球化学;物源;构造背景;四川盆地;荣经地区;地质调查工程

目前,四川盆地下志留统龙马溪组的页岩气勘探开发已取得显著成效,并形成了焦石坝、长宁及威远等页岩气高产气田(王玉满等,2016;聂海宽等,2016;冯动军等,2016;郑志红等,2017;吴安彬等,2020)。为进一步探索龙马溪组潜力资源,四川盆地之外的构造复杂区是目前和下一阶段页岩气勘探开发工作的重点区域(王玉满等,2016,2017;聂海宽等,2016;郑志红等,2017;蒲泊伶等,2020)。荣经位于扬子地台西缘构造复杂区,地处川西南低缓断褶带南缘(冯仁蔚等,2008),多期次构造演化使得区域断裂发育,页岩气富集条件复杂。前期地质调查研究发现,该区与盆地内相似,广泛发育上奥陶统五峰组一下志留统龙马溪组黑色泥页岩,而岩性组合及沉积相带展布又明显与四川盆地内不同(李艳芳等,2015;Ma Yiquan et al., 2016;牟传龙等,2016;Li Yanfang et al., 2017;王玉满等,2017)。同时,该区现有少量页岩气地质研究成果主要集中在龙马溪组的沉积环境、矿物岩石特征、沉积相研究等方面(巩

磊等,2014;牟传龙等,2016;张茜等,2016),而从沉积学及地球化学角度对盆地属性、物源区及构造背景的研究较少,影响了对该区盆地演化历史的整体认识。

沉积盆地中的充填物记录着盆地演化历史中的各种信息,其化学组成受源岩成分、物理化学风化条件、搬运、沉积和成岩作用共同制约(Dickinson, 1985;任军平等,2016)。因此,沉积岩的地球化学特征可以用来分析物源区类型、揭示物源区古风化条件和构造背景,以此来重塑原型盆地类型,讨论大陆地壳演化史和盆山转换关系,为区域构造演化历史提供依据(McLennan et al., 1993; Johnsson, 1993; Andersen, 2005;余谦等,2011)。本文通过对川西南荣经地区志留系龙马溪组泥岩进行系统的岩石矿物学及地球化学特征研究,恢复了龙马溪组泥岩沉积环境、沉积构造背景、古风化作用、古气候条件及源岩属性,初步建立了泥岩与源岩的对应关系。

注:本文为国家科技重大专项“页岩气勘查评价技术试验与应用推广”(编号:2016ZX05034-004)的成果。

收稿日期:2019-08-14;改回日期:2020-07-27;责任编辑:刘志强。Doi:10.16509/j.georeview.2020.05.022

作者简介:张茜,女,1983年生,博士,工程师,主要研究方向为沉积地球化学;Email:76517507@qq.com。

# 1 区域地质特征

受控于加里东运动影响,四川盆地在晚奥陶世—早志留世夹持在东南缘黔中隆起、西缘的康滇古陆以及北缘的川中古隆起之间,形成三隆夹一凹的闭塞海湾沉积格局(严德天等,2008;陈旭等,2014;王玉满等,2016),向西为一深水海槽介于康滇古陆与川中隆起之间连通扬子板块以西的巴颜喀拉洋(梅冥相等,2005;何登发等,2011;李伟等,2014)。荥经地区即位于深水海槽内与板块西缘的大洋连通(图1a)。

荥经地区隶属于上扬子西南边界地带,分布于川西低隆构造带及滇东北冲断褶皱带内(图1b)。受周缘深大断裂围限,总体上呈“两坳夹一隆”的构造形态,北西向展布,隆起部位以前南华系火山岩发育为主(钟勇等,2014;巩磊等,2014;张茜等,2016),坳陷区地层出露较为齐全,缺失前南华系变质岩、石炭系、古近系及新近系,古生界地层较为发育,广泛分布龙马溪组含碳质钙质粉砂质泥岩。但由于经历了加里东运动晚期、海西运动早期以及印

支运动期的构造隆升,龙马溪组部分被剥蚀,厚度不太稳定。

研究区龙马溪组主要分布在雅安荥经县泗坪乡—铅翻沟、天全县鱼泉乡—大井坪、甘孜泸定县冷碛镇—牛背山、荥经县泥巴山—轿顶山一线(图1a、b)。在龙马溪组地层对比图上可以看出(图2),该区龙马溪组自西向东有减薄趋势。大井坪、轿顶山剖面龙马溪组与上覆罗惹坪组灰岩及下伏五峰组硅质岩均呈整合接触,可见观音桥组介壳灰岩(图2,图3a,b)。龙马溪组下段均沉积了深水陆棚相黑色碳质笔石页岩(图3c),页理及水平纹层发育,可见黄铁矿浸染呈星点状或条带状,指示沉积环境为滞留、缺氧的还原环境。上段为浅水陆棚相灰黑色钙质粉砂质泥岩,笔石少见,砂质含量高。其中,富有机质页岩段( $TOC > 1\%$ ;蒲泊伶等,2020)厚度大于40 m,优质页岩段( $TOC > 2\%$ )为10~30 m(图2)。介于它们之间的冷碛剖面、YQ1井、清溪剖面沉积了浅水陆棚相钙质砂质泥岩,未见深水陆棚相沉积,砂质较重、碳酸盐矿物含量较高,白云石发育,富有机质页岩段( $TOC > 1\%$ )小于40 m,未见优质页岩段

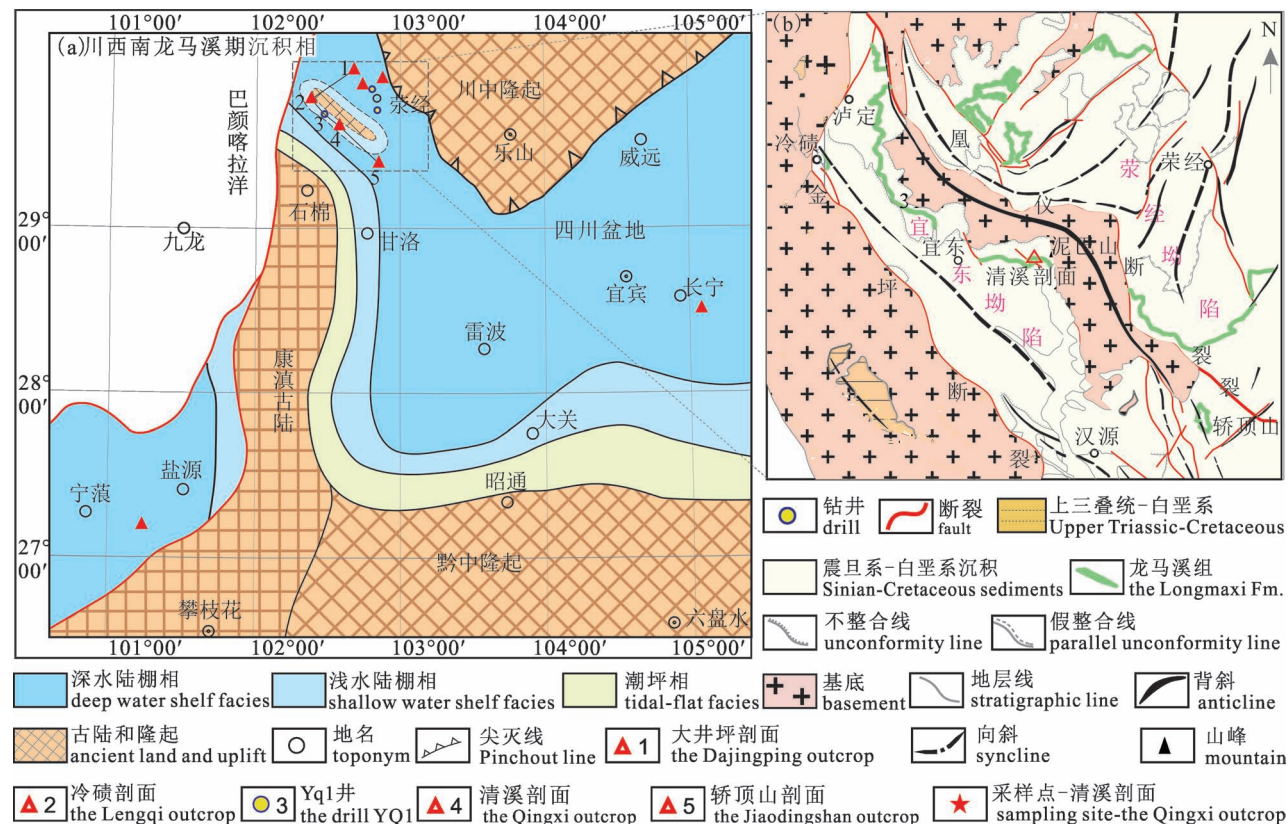


图 1 川西南龙马溪期沉积相图(a, 据牟传龙等, 2016 改编)和荥经地区地质简图(b, 据张茜等, 2016 改编)

Fig. 1 Diagram of depositional facies of the Longmaxi Fm. in southwestern Sichuan (a, modified from Mou Chuanlong et al., 2016&) and geological sketch of the Yingjing area (b, modified from Zhang Qian et al., 2016&)

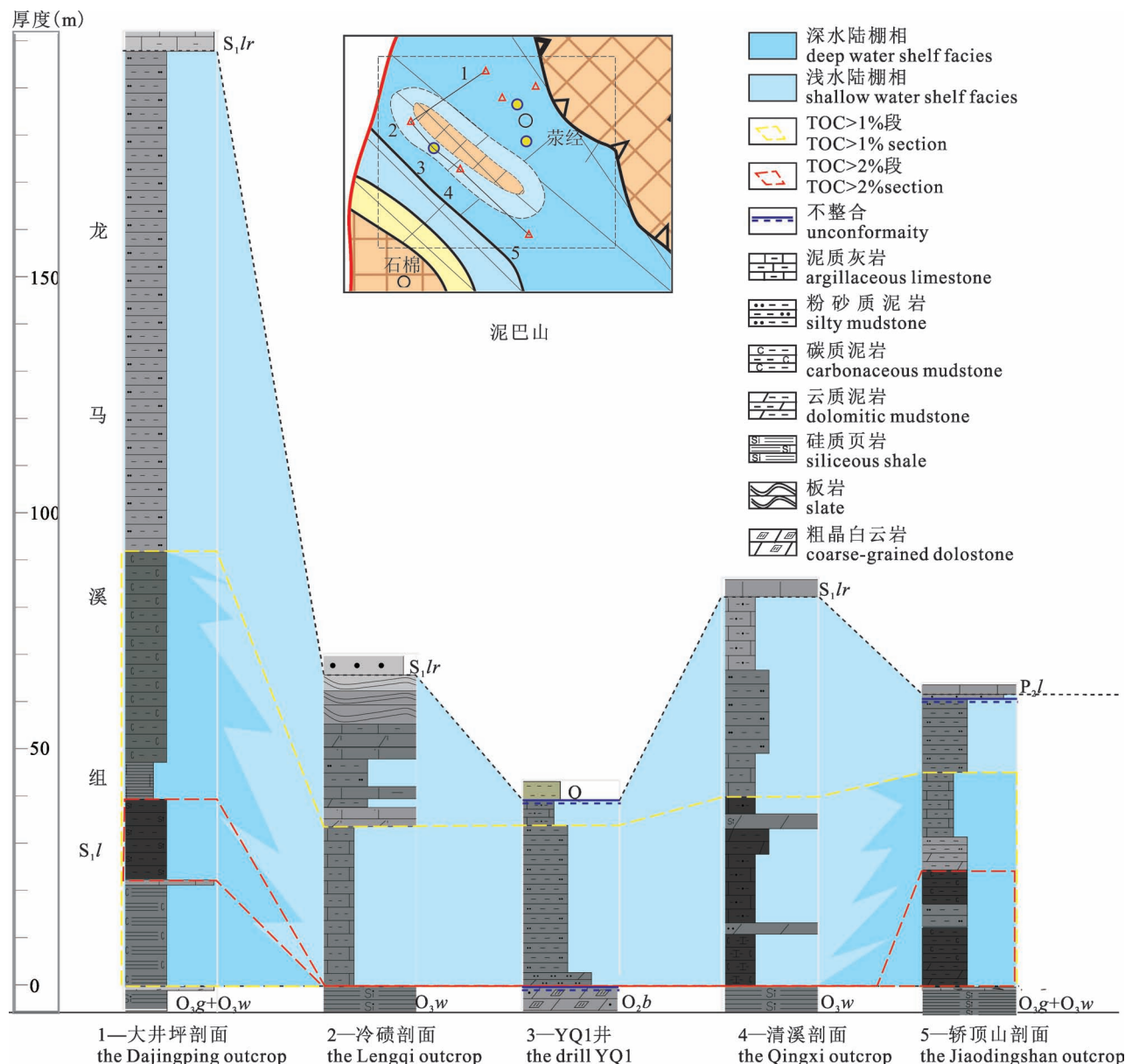


图2 四川盆地荣经地区龙马溪组沉积地层对比图

Fig. 2 Stratigraphic comparison diagram of the Longmaxi Formation in Yingjing area

(TOC>2%;图2)。因此,推测在川中隆起及康滇古陆之间的深水海槽内可能存在小型隆升或水下降起,使得荣经地区龙马溪组沉积期相变较大,岩石非均质性较强,钙质砂质含量较高。

## 2 样品采集与实验方法

此次研究选取区内出露相对较好的清溪剖面系统采样(图1b),该剖面总厚约80 m,与下伏上奥陶统五峰组硅质岩及上覆下志留统罗惹坪组灰岩均呈整合接触。在剖面顶部钻采样井采样,从下往上共采集24件样品作主微量元素分析,其中20件样品

做TOC及矿物成分分析,具体采样位置及编号如图4所示。所有测试均在国土资源部重庆矿产资源监督检测中心完成。分析测试之前,选择新鲜样品在无污染条件下磨碎至粒径小于0.2 mm,用于总有机碳含量分析;磨至200目,用于主量元素和微量元素分析。主量元素使用荷兰帕纳科 Axios mAx PW4400/40X射线荧光光谱仪进行检测,分析误差小于1%。微量及稀土元素使用X-series II电感耦合等离子体质谱仪ICP-MS(美国ThermoFisher)测定,分析误差小于5%。X衍射分析使用ZJ207 Bruker D8 advance型X射线衍射仪,采用Ni滤波

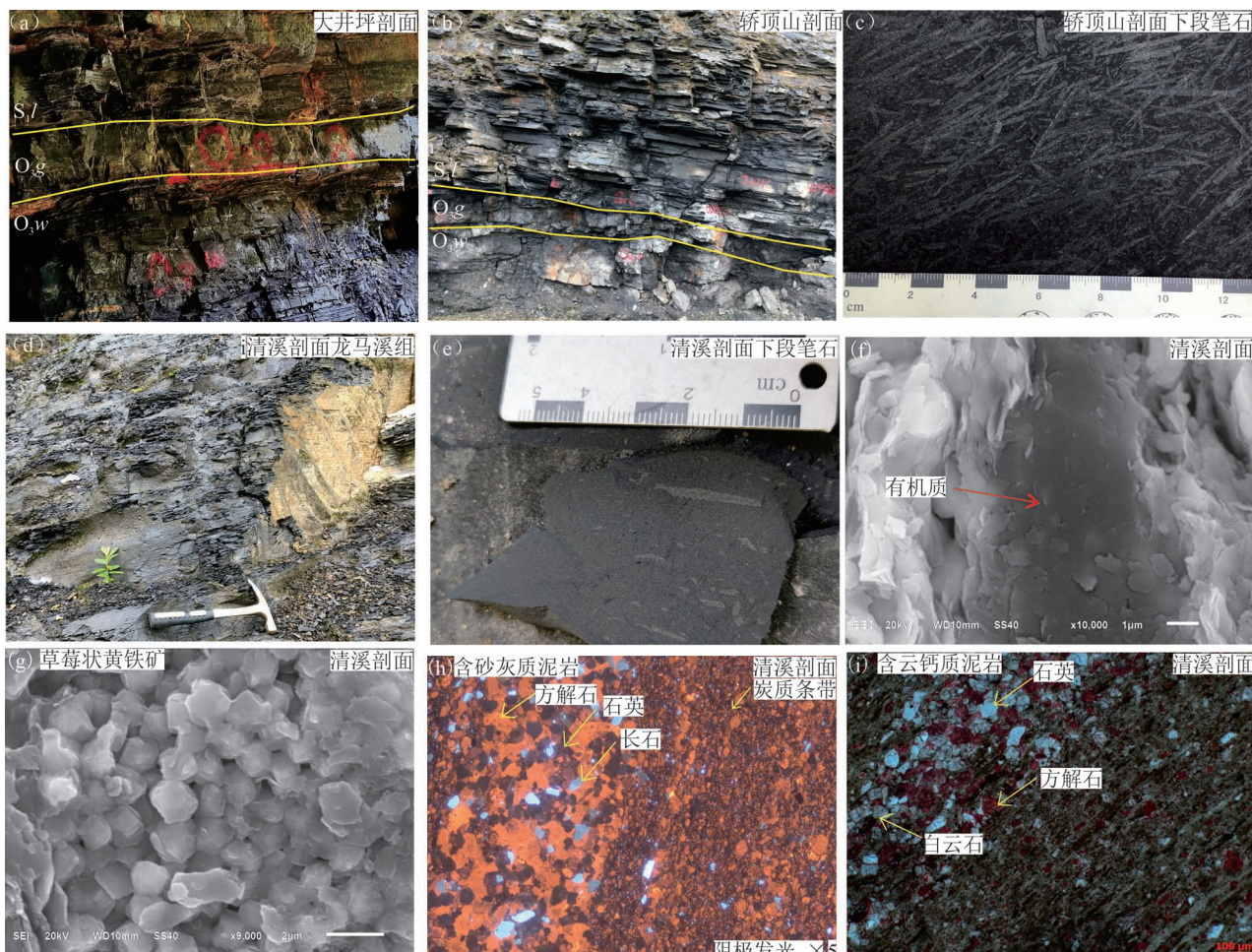


图 3 四川盆地西南缘龙马溪组沉积地层及微观特征: (a) 大井坪剖面宏观照; (b) 轿顶山剖面宏观照; (c) 轿顶山剖面笔石特征照片; (d) 清溪剖面龙马溪组黑色钙质泥岩; (e) 清溪剖面笔石特征照; (f) 清溪剖面有机质, 扫描电镜照片; (g) 清溪剖面草莓状黄铁矿, 扫描电镜照片; (h) 清溪剖面含砂灰质泥岩, 阴极发光照片; (i) 清溪剖面含云钙质泥岩, 薄片特征

Fig. 3 Sedimentary strata and microscopic features of the Longmaxi Fm. on the southwestern margin of the Sichuan Basin: (a) macro photo of the Dajingping profile; (b) macro photo of the Jiaodingshan profile; (c) graptolite photo on the Jiaodingshan outcrop; (d) black calcareous mudstone of the Longmaxi Fm. in the Qingxi outcrop; (e) graptolite photo of the Qingxi outcrop; (f) organic matter of the Qingxi outcrop, SEM; (g) pyrite framboids of the Qingxi outcrop, SEM; (h) silty calcareous mudstone, cathodoluminescence photograph; (i) dolomitic calcareous mudstone of the Qingxi outcrop, thin section characteristics

Cu 靶辐射, 工作电压为 40 kV, 工作电流为 40 mA, 发射狭缝与散射狭缝均为 1°, 接受狭缝 0.3 mm, 扫描方式为步进扫描, 测定标准遵循 SY/T5163—2010, 数据分析采用软件 High Score。

### 3 实验结果

#### 3.1 岩石学及矿物学特征

清溪龙马溪组岩性主要以灰黑色砂质钙质泥岩为主(图 3d), 夹纹层状粉砂质灰岩透镜体, 黄铁矿发育, 笔石等海洋生物少量发育(图 3e), 镜下偶见有机质(图 3f)。薄片特征显示龙马溪组黑色泥岩

整体呈泥质结构, 主要由泥质、方解石组成, 其次为少量的铁质、云母等, 整体具定向性(图 3i)。石英呈粒状不均匀分布, 粒径一般在 0.004~0.10 mm。泥质主要包括黏土矿物和细碎屑。黏土矿物主要为伊利石、高岭石、蒙脱石等的微晶—隐晶质集合体。方解石、白云石呈粒状或以胶结物形式不均匀分布(图 3h,i), 且交代碎屑颗粒边缘成锯齿状, 少量炭质呈条带状分布(图 3h), 砂和粉砂含量一般大于 15%。扫描电镜照片显示黄铁矿晶体呈自形或半自形, 晶粒较细, 多以草莓状集合体形式存在(图 3g), 放射虫等硅质生物少见, 说明其硅质主要为陆源碎

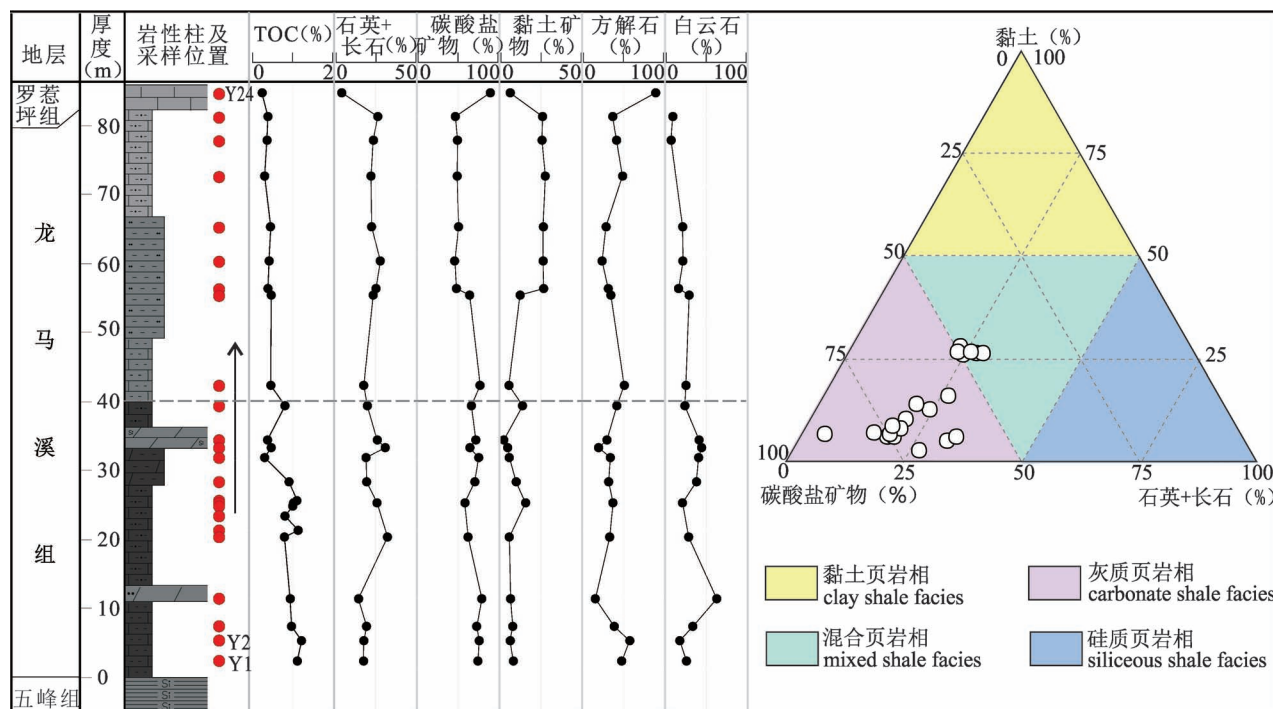


图4 四川盆地清溪剖面矿物岩性柱及采样位置

Fig. 4 Mineral lithological columns and sampling locations of the Qingxi outcrop in the Sichuan Basin

屑硅(张茜等,2018b)。

X衍射定量分析结果显示(表1),岩石主要以碳酸盐矿物、石英和黏土矿物为主,碳酸盐矿物中方解石含量为15.8%~88.9%,平均值为38.7%,白云石含量为7.5%~44.4%,平均值为28.4%,黏土含量为2.6%~37.4%,平均含量为19.51%;石英含量为11.4%~23.3%,平均值为19.5%;长石含量较低,且主要为钾长石,平均含量为4.3%;黄铁矿含量平均为1.6%,大部分手标本中可以观察到。根据页岩岩相划分方案(吴蓝宇等,2016;袁桃等,2020),清溪剖面样品点均投入灰质页岩相及混合质页岩相,指示荣经地区龙马溪组沉积期水体偏浅(王玉满等,2016;吴蓝宇等,2016)。

### 3.2 地球化学特征

清溪剖面龙马溪组TOC含量较低,值为0.2%~1.2%,平均值为0.63%(表2)。主量元素及相关参数

表1 四川盆地清溪剖面龙马溪组矿物成分(%)表

Table 1 Mineral composition of the Longmaxi Fm. (%) of the Qingxi outcrop in the Sichuan Basin

| 样品编号 | TOC  | 石英   | 钾长石 | 斜长石 | 方解石  | 白云石  | 黄铁矿 | 石英+长石 | 碳酸盐矿物 | 黏土矿物 |
|------|------|------|-----|-----|------|------|-----|-------|-------|------|
| Y24  | 0.26 | 3.6  |     | 1   | 88.9 |      |     | 4.6   | 88.9  | 6.5  |
| Y23  | 0.4  | 23.3 | 2.1 |     | 37.0 | 9.6  | 1   | 26.4  | 46.6  | 26.0 |
| Y22  | 0.38 | 21.5 | 2.3 |     | 41.6 | 7.5  |     | 23.8  | 49.1  | 25.7 |
| Y21  | 0.32 | 20.3 | 0.9 | 0.4 | 48.9 |      | 0.7 | 22.3  | 48.9  | 27.6 |
| Y20  | 0.46 | 20.3 | 1.8 |     | 28.9 | 21.5 | 0.6 | 22.7  | 50.4  | 26.5 |
| Y19  | 0.43 | 21.9 | 3.1 | 0.3 | 24.0 | 21.7 | 2.6 | 27.9  | 45.7  | 26.4 |
| Y18  | 0.4  | 19.5 | 2.3 |     | 31.5 | 16.5 | 3.5 | 25.3  | 48.0  | 26.7 |
| Y17  | 0.48 | 16.2 | 4.7 | 1   | 34.6 | 29.3 | 1.7 | 23.6  | 63.9  | 12.5 |
| Y16  | 0.47 | 11.0 | 5.1 |     | 50.9 | 25.5 | 1.8 | 17.9  | 76.4  | 5.7  |
| Y15  | 0.81 | 12.9 | 3.7 |     | 41.8 | 24.2 | 3.5 | 20.1  | 66.0  | 13.9 |
| Y14  | 0.39 | 18.9 | 6.4 |     | 29.9 | 41.4 | 0.8 | 26.1  | 71.3  | 2.6  |
| Y13  | 0.48 | 21.3 | 9.3 |     | 19.8 | 44.4 | 0.3 | 30.9  | 64.2  | 4.9  |
| Y12  | 0.32 | 13.8 | 5.5 |     | 34.0 | 40.8 |     | 19.3  | 74.8  | 5.9  |
| Y11  | 0.91 | 12.4 | 5.4 |     | 32.0 | 38.2 | 1.9 | 19.7  | 70.2  | 10.1 |
| Y9   | 1.02 | 20.9 | 3.0 | 0.6 | 37.1 | 21.2 | 1.4 | 25.9  | 58.3  | 15.8 |
| Y5   | 0.8  | 23.5 | 6.0 |     | 33.2 | 28.7 | 2.7 | 32.2  | 61.9  | 5.9  |
| Y4   | 0.94 | 8.7  | 5.4 |     | 15.8 | 62.7 | 0.7 | 14.8  | 78.5  | 6.7  |
| Y3   | 0.97 | 11.4 | 5.4 |     | 38.7 | 33.7 | 2.8 | 19.6  | 72.4  | 8.0  |
| Y2   | 1.21 | 12.7 | 5.0 |     | 57.5 | 18.0 | 0.3 | 18.0  | 75.5  | 6.5  |
| Y1   | 1.11 | 11.5 | 4.8 |     | 47.7 | 26.1 | 1.5 | 17.8  | 73.8  | 8.4  |
| 平均值  | 0.63 | 16.3 | 4.3 | 0.7 | 38.7 | 28.4 | 1.6 | 21.9  | 64.2  | 13.6 |

结果如表 2 所示,  $\text{SiO}_2$  含量整体较低, 值为 20.66% ~ 45.04%, 均值为 34%。 $\text{Al}_2\text{O}_3$  含量为 4.18% ~ 14.71%, 平均为 8.24%, 从底到顶值增大, 说明到龙马溪晚期陆源碎屑输入量逐渐增大 (Zhou Lian et al., 2015; 王玉满等, 2017)。CaO 含量较高, 值为 13.89% ~ 30.41%, 均值为 21.40%,  $\text{MgO}$  含量为 2.11% ~ 10.06%, 平均为 4.53%, CaO 含量高于  $\text{MgO}$  含量, 说明泥岩中方解石丰度大于白云石丰度。 $\text{K}_2\text{O}$  含量变化较小, 值为 2.16% ~ 5.13%, 平均值为 3.29%;  $\text{Na}_2\text{O}$  含量为 0.089% ~ 0.15%, 平均值为 0.12%;  $\text{P}_2\text{O}_5$  值为 0.061% ~ 0.4%, 平均值为 0.13%;  $\text{TiO}_2$  值为 0.17% ~ 0.43%, 平均值为 0.30%;  $\text{MnO}$  含量为 0.023% ~ 0.051%, 平均值为 0.036%。烧失量 (LOI) 较高, 平均值为 24.51%, 与样品中碳酸盐矿物含量较高相关。相对于澳大利亚后太古宙平均页岩 PAAS (Taylor and McLennan, 1985),  $\text{SiO}_2$ 、 $\text{Al}_2\text{O}_3$  明显亏损 (样品/PAAS 值分别

为 0.54、0.44), 而  $\text{CaO}$  和  $\text{MgO}$  明显富集 (样品/PAAS 值分别为 11.26、2.07)。

Mo、U、V、Co、Ni、Cu、Zn 等微量元素不仅对水体的氧化还原环境较为敏感, 同时还是重要的营养元素参于生物代谢与生化过程 (Algeo et al., 2009; Tribouillard et al., 2012)。因此它们的富集程度常用来指示水体的氧化还原性及初级古生产力 (Tribouillard et al., 2012; Zhou Lian et al., 2015)。研究区 Mo、U、V、Co、Ni、Cu、Zn 含量与 PAAS 值相近 (表 3), Mo、U、V、Ni 呈现弱富集或不富集特征 (样品/PAAS 值分别为 1.13、1.02、1.55), Co、Cu、Zn 显示弱的亏损 (样品/PAAS 值分别为 0.83、0.85、0.61), 指示研究区龙马溪组沉积水体还原性较弱, 初级古生产力较低 (Zhou Lian et al., 2015; Ma Yiquan et al., 2016; 张茜等, 2016; Li Yanfang et al., 2017)。高场强元素 Th、Zr、Y 的平均含量分别是  $10.9 \times 10^{-6}$ 、 $93.12 \times 10^{-6}$ 、 $18.7 \times 10^{-6}$ , 相对于

表 2 四川盆地清溪剖面主量元素含量 (%) 及相关参数特征

Table 2 Contents of major elements(%) and some associated parameters of the Qingxi outcrop in the Sichuan Basin

| 样品        | $\text{SiO}_2$ | $\text{Al}_2\text{O}_3$ | $\text{Fe}_2\text{O}_3$ | $\text{MgO}$ | CaO   | $\text{Na}_2\text{O}$ | $\text{K}_2\text{O}$ | MnO   | $\text{TiO}_2$ | $\text{P}_2\text{O}_5$ | 烧失量   | $\text{Al}_2\text{O}_3/\text{TiO}_2$ | $\text{TiO}_2/\text{Zr}$ | CIA | ICV  |
|-----------|----------------|-------------------------|-------------------------|--------------|-------|-----------------------|----------------------|-------|----------------|------------------------|-------|--------------------------------------|--------------------------|-----|------|
| y1        | 23.9           | 5.31                    | 2.03                    | 4.74         | 29.78 | 0.1                   | 2.93                 | 0.034 | 0.22           | 0.08                   | 30.2  | 24.14                                | 22.45                    | 58  | 2.64 |
| y2        | 23.6           | 5.78                    | 1.92                    | 2.11         | 30.41 | 0.12                  | 2.6                  | 0.025 | 0.22           | 0.09                   | 32.2  | 26.27                                | 24.89                    | 62  | 1.27 |
| y3        | 21.3           | 4.41                    | 1.50                    | 4.29         | 30.15 | 0.11                  | 2.19                 | 0.028 | 0.17           | 0.08                   | 33.9  | 25.94                                | 15.60                    | 59  | 2.84 |
| y4        | 20.7           | 4.31                    | 1.74                    | 10.06        | 25.54 | 0.11                  | 2.16                 | 0.034 | 0.17           | 0.09                   | 35.8  | 25.35                                | 16.83                    | 59  | 6.35 |
| y5        | 37.5           | 5.42                    | 2.57                    | 4.7          | 21.26 | 0.11                  | 2.77                 | 0.023 | 0.25           | 0.40                   | 25.3  | 21.68                                | 15.43                    | 59  | 2.65 |
| y6        | 39.5           | 8.06                    | 2.62                    | 5.19         | 17.08 | 0.13                  | 3.96                 | 0.026 | 0.32           | 0.28                   | 22.1  | 25.19                                | 30.77                    | 61  | 1.96 |
| y7        | 35.7           | 7.83                    | 2.59                    | 3.63         | 20.84 | 0.12                  | 3.53                 | 0.027 | 0.3            | 0.13                   | 25.2  | 26.10                                | 39.42                    | 63  | 1.50 |
| y8        | 37.0           | 8.42                    | 2.76                    | 3.67         | 20.53 | 0.089                 | 3.92                 | 0.025 | 0.33           | 0.12                   | 24.6  | 25.52                                | 41.04                    | 62  | 1.41 |
| y9        | 36.3           | 7.38                    | 2.68                    | 4.96         | 19.27 | 0.14                  | 3.55                 | 0.028 | 0.29           | 0.17                   | 24.8  | 25.45                                | 27.88                    | 61  | 2.06 |
| y10       | 29.1           | 5.75                    | 2.07                    | 5.58         | 24.31 | 0.11                  | 2.62                 | 0.029 | 0.22           | 0.15                   | 29.2  | 26.14                                | 26.70                    | 62  | 2.82 |
| y11       | 28.2           | 5.71                    | 1.98                    | 5.96         | 25.2  | 0.11                  | 2.77                 | 0.028 | 0.23           | 0.24                   | 29.6  | 24.83                                | 27.48                    | 61  | 3.00 |
| y12       | 29.8           | 4.18                    | 1.52                    | 5.46         | 25.52 | 0.15                  | 2.42                 | 0.030 | 0.18           | 0.22                   | 29.2  | 23.22                                | 10.29                    | 55  | 3.75 |
| y13       | 28.6           | 5.08                    | 3.03                    | 9.64         | 21.36 | 0.14                  | 2.67                 | 0.041 | 0.25           | 0.10                   | 28.5  | 20.32                                | 19.84                    | 58  | 5.38 |
| y14       | 29.8           | 7.83                    | 3.03                    | 3.81         | 24.76 | 0.13                  | 2.89                 | 0.034 | 0.28           | 0.11                   | 25.6  | 27.96                                | 42.42                    | 67  | 1.59 |
| y15       | 27.4           | 6.4                     | 2.51                    | 3.98         | 28.66 | 0.13                  | 2.7                  | 0.038 | 0.23           | 0.09                   | 27.8  | 27.87                                | 40.78                    | 63  | 1.95 |
| y16       | 44.5           | 14.7                    | 5.35                    | 3.56         | 12.13 | 0.12                  | 5.13                 | 0.043 | 0.49           | 0.10                   | 14.4  | 30.02                                | 63.55                    | 69  | 0.92 |
| y17       | 34.7           | 8.06                    | 3.76                    | 3.52         | 22.01 | 0.13                  | 2.88                 | 0.047 | 0.27           | 0.09                   | 24.6  | 29.85                                | 31.95                    | 67  | 1.52 |
| y18       | 41.3           | 11.8                    | 4.34                    | 3.73         | 16.71 | 0.092                 | 4.14                 | 0.042 | 0.39           | 0.10                   | 18.5  | 30.13                                | 52.14                    | 69  | 1.12 |
| y19       | 40.3           | 11.0                    | 4.45                    | 3.76         | 16.89 | 0.14                  | 3.33                 | 0.045 | 0.32           | 0.10                   | 19.2  | 34.34                                | 38.37                    | 71  | 1.22 |
| y20       | 45.0           | 12.1                    | 4.83                    | 3.72         | 13.89 | 0.12                  | 4.09                 | 0.045 | 0.38           | 0.12                   | 15.6  | 31.84                                | 43.93                    | 69  | 1.12 |
| y21       | 40.6           | 11.4                    | 4.23                    | 3.77         | 16.46 | 0.15                  | 3.65                 | 0.050 | 0.36           | 0.08                   | 17.9  | 31.53                                | 39.69                    | 70  | 1.18 |
| y22       | 40.5           | 12.7                    | 4.61                    | 2.43         | 17.48 | 0.11                  | 4.05                 | 0.051 | 0.43           | 0.06                   | 18.0  | 29.51                                | 64.56                    | 71  | 0.80 |
| y23       | 39.4           | 11.6                    | 4.68                    | 3.25         | 18.31 | 0.13                  | 3.95                 | 0.045 | 0.38           | 0.09                   | 18.8  | 30.47                                | 48.41                    | 69  | 1.06 |
| y24       | 41.5           | 12.5                    | 4.59                    | 3.11         | 15    | 0.13                  | 4.03                 | 0.046 | 0.4            | 0.07                   | 17.4  | 31.35                                | 49.69                    | 70  | 0.95 |
| 均值        | 34.00          | 8.24                    | 3.14                    | 4.53         | 21.40 | 0.12                  | 3.29                 | 0.04  | 0.30           | 0.13                   | 24.51 | 27.29                                | 34.76                    | 64  | 2.13 |
| PAAS 值    | 62.80          | 18.90                   | 7.18                    | 2.19         | 1.90  | 1.19                  | 3.68                 | 0.11  | 0.99           | 0.16                   |       |                                      |                          |     |      |
| 均值/PAAS 值 | 0.54           | 0.44                    | 0.44                    | 2.07         | 11.26 | 0.10                  | 0.89                 | 0.33  | 0.30           | 0.83                   |       |                                      |                          |     |      |

表3 四川盆地清溪剖面微量元素含量( $\times 10^{-6}$ )及相关参数

Table 3 Contents of trace elements ( $\times 10^{-6}$ ) and related parameters of the Qingxi outcrop in the Sichuan Basin

| 样品编号      | Mo   | U    | V     | Co    | Ni    | Cu    | Zn    | Cr    | Th    | Y     | Sc    | Rb     | Zr     | $\frac{\text{Th}}{\text{U}}$ | $\frac{\text{Rb}}{\text{Sr}}$ | $\frac{\text{La}}{\text{Th}}$ | $\frac{\text{Sc}}{\text{Gr}}$ | $\frac{\text{La}}{\text{Sc}}$ | $\frac{\text{Co}}{\text{Th}}$ |
|-----------|------|------|-------|-------|-------|-------|-------|-------|-------|-------|-------|--------|--------|------------------------------|-------------------------------|-------------------------------|-------------------------------|-------------------------------|-------------------------------|
| Y1        | 2.28 | 2.61 | 20.7  | 5.92  | 19.50 | 21.90 | 15.90 | 20.70 | 8.39  | 12.40 | 4.95  | 64.50  | 98.00  | 13.63                        | 0.27                          | 2.63                          | 0.24                          | 14.60                         | 3.47                          |
| Y2        | 2.56 | 3.01 | 20.9  | 4.90  | 18.50 | 23.50 | 21.50 | 15.20 | 6.89  | 13.10 | 5.19  | 65.70  | 88.40  | 13.78                        | 0.26                          | 2.09                          | 0.34                          | 24.58                         | 1.56                          |
| Y3        | 1.32 | 1.22 | 17.9  | 2.85  | 10.70 | 10.40 | 60.80 | 17.00 | 4.48  | 7.20  | 2.39  | 55.70  | 109.00 | 7.84                         | 0.22                          | 2.83                          | 0.14                          | 16.03                         | 3.66                          |
| Y4        | 1.92 | 2.25 | 26.2  | 4.67  | 16.20 | 17.90 | 22.90 | 20.70 | 7.59  | 11.70 | 4.15  | 57.40  | 101.00 | 13.02                        | 0.44                          | 2.60                          | 0.20                          | 16.52                         | 7.86                          |
| Y5        | 3.12 | 3.38 | 67.9  | 5.37  | 32.00 | 17.20 | 13.10 | 38.40 | 10.70 | 27.20 | 5.21  | 72.70  | 162.00 | 32.64                        | 0.43                          | 3.37                          | 0.14                          | 12.87                         | 3.45                          |
| Y6        | 2.67 | 3.28 | 111.0 | 7.41  | 39.10 | 24.00 | 147.8 | 58.40 | 11.40 | 22.40 | 7.63  | 104.00 | 104.00 | 27.29                        | 0.69                          | 2.56                          | 0.13                          | 17.66                         | 2.51                          |
| Y7        | 2.03 | 2.78 | 65.8  | 7.93  | 35.70 | 21.70 | 27.2  | 48.50 | 10.90 | 19.60 | 8.01  | 102.00 | 76.10  | 24.08                        | 0.51                          | 2.79                          | 0.17                          | 15.75                         | 1.96                          |
| Y8        | 2.18 | 2.81 | 81.6  | 8.27  | 35.50 | 23.30 | 30.6  | 55.10 | 10.80 | 19.00 | 8.14  | 110.00 | 80.40  | 23.36                        | 0.59                          | 2.80                          | 0.15                          | 15.59                         | 1.86                          |
| Y9        | 2.57 | 3.04 | 98.2  | 7.05  | 35.00 | 22.70 | 22.9  | 60.50 | 10.40 | 21.00 | 6.92  | 97.80  | 104.00 | 25.46                        | 0.60                          | 2.76                          | 0.11                          | 16.27                         | 2.78                          |
| Y10       | 2.17 | 2.67 | 53.5  | 5.62  | 30.30 | 18.00 | 32.7  | 33.20 | 8.58  | 19.50 | 5.63  | 72.90  | 82.40  | 23.88                        | 0.38                          | 3.08                          | 0.17                          | 17.22                         | 3.58                          |
| Y11       | 2.01 | 3.17 | 60.4  | 5.15  | 30.70 | 16.70 | 93.8  | 36.90 | 8.15  | 22.90 | 5.64  | 71.70  | 83.70  | 29.04                        | 0.38                          | 3.44                          | 0.15                          | 16.46                         | 3.71                          |
| Y12       | 1.60 | 3.48 | 45.4  | 3.22  | 20.60 | 12.70 | 10.0  | 25.50 | 9.16  | 20.60 | 3.19  | 59.30  | 174.90 | 25.06                        | 0.35                          | 2.74                          | 0.13                          | 17.07                         | 4.59                          |
| Y13       | 2.08 | 2.54 | 76.4  | 4.22  | 22.80 | 14.50 | 13.4  | 39.90 | 8.80  | 14.20 | 4.44  | 72.10  | 126.00 | 17.27                        | 0.50                          | 2.30                          | 0.11                          | 15.04                         | 6.32                          |
| Y14       | 1.90 | 3.25 | 57.3  | 8.76  | 36.60 | 20.70 | 23.0  | 41.10 | 11.20 | 18.80 | 8.20  | 99.00  | 66.00  | 22.90                        | 0.34                          | 2.63                          | 0.20                          | 18.00                         | 1.96                          |
| Y15       | 1.26 | 2.21 | 39.9  | 6.51  | 25.40 | 13.40 | 19.3  | 28.60 | 7.79  | 15.70 | 6.07  | 82.80  | 56.40  | 19.44                        | 0.32                          | 3.22                          | 0.21                          | 16.84                         | 2.39                          |
| Y16       | 0.41 | 3.29 | 87.0  | 13.80 | 38.60 | 29.00 | 45.9  | 78.20 | 17.9  | 18.70 | 14.90 | 191.00 | 77.10  | 22.06                        | 1.06                          | 2.53                          | 0.19                          | 15.22                         | 1.31                          |
| Y17       | 4.11 | 2.71 | 59.0  | 9.49  | 38.10 | 22.20 | 41.6  | 45.10 | 11.0  | 19.00 | 8.53  | 102.00 | 84.50  | 22.69                        | 0.39                          | 2.84                          | 0.19                          | 18.87                         | 1.95                          |
| Y18       | 0.69 | 2.89 | 65.1  | 10.5  | 33.90 | 23.40 | 38.1  | 58.90 | 13.2  | 20.70 | 11.30 | 145.00 | 74.80  | 24.77                        | 0.60                          | 2.87                          | 0.19                          | 17.79                         | 1.44                          |
| Y19       | 0.85 | 2.59 | 65.6  | 12.0  | 36.00 | 24.20 | 71.4  | 51.40 | 13.3  | 21.00 | 11.40 | 135.00 | 83.40  | 25.05                        | 0.57                          | 2.79                          | 0.22                          | 21.21                         | 1.60                          |
| Y20       | 0.62 | 2.68 | 75.8  | 12.7  | 39.00 | 28.20 | 49.8  | 62.80 | 14.7  | 22.30 | 12.50 | 153.00 | 86.50  | 26.27                        | 0.69                          | 2.73                          | 0.20                          | 18.87                         | 1.48                          |
| Y21       | 0.52 | 2.97 | 64.5  | 12.2  | 34.40 | 23.10 | 47.2  | 56.80 | 13.7  | 21.50 | 11.70 | 139.00 | 90.70  | 25.37                        | 0.66                          | 2.74                          | 0.21                          | 19.83                         | 1.49                          |
| Y22       | 0.90 | 2.77 | 64.2  | 13.7  | 39.30 | 26.30 | 71.8  | 56.70 | 14.7  | 17.90 | 13.00 | 155.00 | 66.60  | 21.25                        | 0.87                          | 2.71                          | 0.23                          | 15.06                         | 1.05                          |
| Y23       | 0.53 | 2.64 | 64.9  | 11.9  | 35.60 | 26.10 | 64.8  | 59.00 | 13.0  | 19.90 | 11.30 | 143.00 | 78.50  | 23.64                        | 0.48                          | 2.75                          | 0.19                          | 18.42                         | 1.41                          |
| Y24       | 0.52 | 2.83 | 75.1  | 14.2  | 41.40 | 30.30 | 51.2  | 61.90 | 14.8  | 21.20 | 13.20 | 157.00 | 80.50  | 25.27                        | 0.58                          | 2.79                          | 0.21                          | 17.39                         | 1.19                          |
| 平均值       | 1.70 | 2.79 | 61.01 | 8.26  | 31.04 | 21.31 | 43.20 | 44.60 | 10.9  | 18.65 | 8.07  | 104.48 | 93.12  | 22.30                        | 0.51                          | 2.77                          | 0.18                          | 17.21                         | 2.69                          |
| PAAS值     | 1.5  | 2.8  | 60    | 10    | 20    | 25    | 71    | 35    | 10.7  | 27    | 14    | 112    | 190    |                              |                               |                               |                               |                               |                               |
| 平均值/PAAS值 | 1.13 | 1.00 | 1.02  | 0.83  | 1.55  | 0.85  | 0.61  | 1.27  | 1.02  | 0.69  | 0.58  | 0.93   | 0.49   |                              |                               |                               |                               |                               |                               |

PAAS, Th 弱富集而 Zr、Y 显示亏损(样品/PAAS 值分别为 1.02、0.49、0.69) (Taylor and McLennan, 1985), 高场强元素受化学风化的影响相对较小, 可以代表沉积物源区的特征(王启宇等, 2018)。

清溪剖面稀土元素总量  $\Sigma\text{REE}$  为  $53.2 \times 10^{-6} \sim 183 \times 10^{-6}$ , 均值为  $131.1 \times 10^{-6}$ , 略低于北美平均页岩 NASC ( $167.4 \times 10^{-6}$ ) (Haskin et al., 1968), 与范德廉等(1987)总结的 87 个黑色岩层中的泥质岩的稀土元素总量 ( $132 \times 10^{-6} \sim 334 \times 10^{-6}$ ) 接近。LREE/HREE 值反映了轻、重稀土元素的分馏程度, 比值越大表明 LREE 越富集,  $\Sigma\text{LREE}/\Sigma\text{HREE}$  为  $7.20 \times 10^{-6} \sim 11.14 \times 10^{-6}$ , 平均值为  $8.98 \times 10^{-6}$ , 显示轻稀土相对重稀土元素明显富集。 $\text{La}_N/\text{Yb}_N$  (N 表示球粒陨石标准化, 下同) 值受陆源环境影响较大, 一般随着陆源碎屑输入的减少,  $\text{La}_N/\text{Yb}_N$  有规律的递减(杜远生等, 2007)。研究区龙马溪组泥岩  $\text{La}_N/\text{Yb}_N$  值为

1.07~1.97, 平均值为 1.60, 指示其受大陆边缘碎屑物质影响较大, 靠近陆缘或沉积期水体相对较浅。样品 Eu 异常  $\delta\text{Eu}_N = 0.60 \sim 0.67$ , 平均 0.64, 为明显 Eu 负异常, 暗示其来自酸性花岗岩区的物质可能较多(Bai Yueyue et al., 2015; 张茜等, 2018a);  $\delta\text{Ce}_S = 0.80 \sim 0.94$ , 平均 0.85 (S 为 PAAS 标准化, 下同), 显示弱负异常, 指示沉积水体为弱的还原环境(张茜等, 2018a)。

## 4 讨论

### 4.1 物源分析

研究发现, 成岩作用会影响沉积岩的化学成分(Shields and Stille, 2001), 因此, 在应用化学成分特征判定其物源属性前应先进行成岩作用研究, 同时应尽量结合多种化学参数共同判定(张建军等, 2017)。碎屑沉积岩的稀土元素特征可作为其成岩

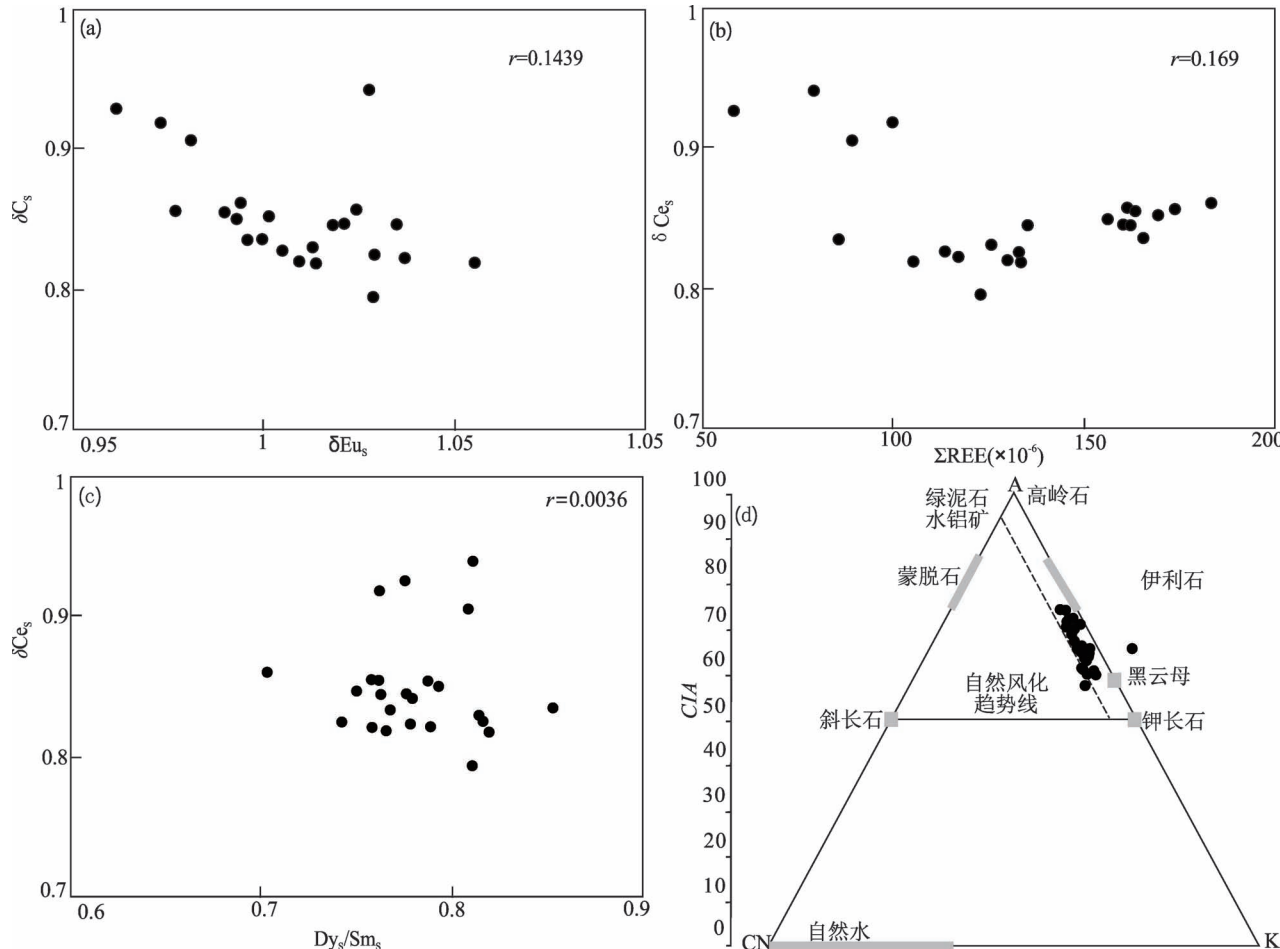


图 5 四川盆地清溪剖面  $\delta\text{Ce}_S-\delta\text{Eu}_N$ (a)、 $\delta\text{Ce}_S-\Sigma\text{REE}$ (b)、 $\delta\text{Ce}_S-\text{Dy}_S/\text{Sm}_S$ (c) 及 A-CN-K(d) 图解  
(底图据 Sensarma et al., 2008)

Fig. 5  $\delta\text{Ce}_S-\delta\text{Eu}_N$ (a),  $\delta\text{Ce}_S-\Sigma\text{REE}$ (b),  $\delta\text{Ce}_S-\text{Dy}_S/\text{Sm}_S$ (c) and A-CN-K (d) diagrams of the Qingxi outcrop in the Sichuan Basin (base map from Sensarma et al., 2008)

表 4 四川盆地清溪剖面稀土元素及相关参数特征( $\times 10^{-6}$ )

Table 4 REE and related parameters of Qingxi outcrop in the Sichuan Basin ( $\times 10^{-6}$ )

| 编号  | Ia    | Ce    | Pr   | Nd    | Sm   | Eu   | Gd   | Tb   | Dy   | Ho   | Er   | Tm   | Yb   | Lu   | $\Sigma$ REE | L/R  | $\delta$ Eu <sub>N</sub> | $\delta$ Eus | $\delta$ Ce <sub>S</sub> | $\delta$ La/S | $\delta$ Yb <sub>S</sub> | $\frac{\delta$ La}{ $\delta$ Sm <sub>S</sub> } | $\frac{\delta$ La}{ $\delta$ Yb <sub>S</sub> } |
|-----|-------|-------|------|-------|------|------|------|------|------|------|------|------|------|------|--------------|------|--------------------------|--------------|--------------------------|---------------|--------------------------|--|--|
| Y1  | 22.1  | 40.2  | 4.84 | 18.2  | 3.34 | 0.66 | 3.04 | 0.48 | 2.5  | 0.48 | 1.45 | 0.2  | 1.26 | 0.19 | 98.9         | 9.3  | 0.62                     | 0.97         | 0.91                     | 1.65          | 0.76                     | 1.35   | 1.78   |
| Y2  | 14.4  | 30.3  | 4.03 | 16.2  | 3.2  | 0.67 | 2.93 | 0.46 | 2.55 | 0.49 | 1.46 | 0.21 | 1.27 | 0.19 | 78.4         | 7.2  | 0.66                     | 1.02         | 0.95                     | 1.07          | 0.81                     | 2.11   | 1.10   |
| Y3  | 12.7  | 23.3  | 2.78 | 10.7  | 1.89 | 0.37 | 1.73 | 0.27 | 1.44 | 0.29 | 0.78 | 0.11 | 0.74 | 0.1  | 57.2         | 9.5  | 0.61                     | 0.95         | 0.92                     | 1.62          | 0.78                     | 2.37   | 1.76   |
| Y4  | 19.7  | 35.7  | 4.41 | 16.3  | 2.97 | 0.61 | 2.87 | 0.43 | 2.36 | 0.45 | 1.35 | 0.18 | 1.21 | 0.18 | 88.7         | 8.8  | 0.63                     | 0.97         | 0.90                     | 1.54          | 0.81                     | 1.30   | 1.68   |
| Y5  | 36.1  | 62.2  | 8.61 | 33.5  | 6.13 | 1.26 | 5.76 | 0.88 | 4.62 | 0.87 | 2.42 | 0.32 | 2.02 | 0.28 | 165.0        | 8.6  | 0.64                     | 0.99         | 0.83                     | 1.69          | 0.77                     | 0.59   | 1.33   |
| Y6  | 29.2  | 49.2  | 6.84 | 26.6  | 4.95 | 1.03 | 4.46 | 0.7  | 3.79 | 0.75 | 2.14 | 0.29 | 1.93 | 0.26 | 132.1        | 8.2  | 0.66                     | 1.02         | 0.82                     | 1.43          | 0.78                     | 0.58   | 1.30   |
| Y7  | 30.4  | 50.1  | 6.88 | 26.4  | 4.79 | 0.99 | 4.39 | 0.66 | 3.6  | 0.7  | 1.99 | 0.29 | 1.73 | 0.26 | 133.2        | 8.8  | 0.65                     | 1.01         | 0.81                     | 1.66          | 0.76                     | 0.69   | 1.55   |
| Y8  | 30.2  | 49.2  | 6.65 | 25.1  | 4.56 | 0.94 | 4.19 | 0.62 | 3.4  | 0.66 | 1.9  | 0.27 | 1.74 | 0.24 | 129.7        | 9.0  | 0.65                     | 1.00         | 0.81                     | 1.64          | 0.76                     | 0.68   | 1.59   |
| Y9  | 28.7  | 49.3  | 6.97 | 27    | 5.17 | 0.98 | 4.64 | 0.69 | 3.77 | 0.71 | 2.03 | 0.28 | 1.73 | 0.26 | 132.2        | 8.4  | 0.60                     | 0.93         | 0.82                     | 1.56          | 0.74                     | 0.67   | 1.37   |
| Y10 | 26.4  | 43.6  | 5.96 | 22.9  | 4.26 | 0.9  | 3.9  | 0.6  | 3.3  | 0.63 | 1.87 | 0.25 | 1.64 | 0.23 | 116.4        | 8.4  | 0.66                     | 1.03         | 0.82                     | 1.52          | 0.79                     | 0.92   | 1.35   |
| Y11 | 28    | 44.6  | 6.3  | 24.3  | 4.56 | 0.97 | 4.3  | 0.66 | 3.63 | 0.71 | 2.05 | 0.28 | 1.75 | 0.25 | 122.4        | 8.0  | 0.66                     | 1.02         | 0.79                     | 1.51          | 0.81                     | 0.90   | 1.22   |
| Y12 | 25.1  | 42    | 5.76 | 22.3  | 4.28 | 0.89 | 4.04 | 0.62 | 3.43 | 0.69 | 1.98 | 0.27 | 1.74 | 0.26 | 113.4        | 7.7  | 0.64                     | 1.00         | 0.82                     | 1.36          | 0.82                     | 1.02   | 1.22   |
| Y13 | 20.2  | 32.3  | 4.11 | 15.4  | 2.83 | 0.59 | 2.71 | 0.41 | 2.37 | 0.49 | 1.46 | 0.21 | 1.41 | 0.2  | 84.7         | 8.1  | 0.64                     | 0.99         | 0.82                     | 1.35          | 0.85                     | 1.06   | 1.42   |
| Y14 | 29.5  | 48    | 6.32 | 23.6  | 4.2  | 0.88 | 3.96 | 0.6  | 3.36 | 0.66 | 1.94 | 0.27 | 1.79 | 0.26 | 125.3        | 8.8  | 0.65                     | 1.00         | 0.82                     | 1.55          | 0.81                     | 0.84   | 1.57   |
| Y15 | 25.1  | 39.8  | 5.24 | 19.6  | 3.53 | 0.76 | 3.24 | 0.51 | 2.84 | 0.55 | 1.62 | 0.23 | 1.43 | 0.2  | 104.7        | 8.9  | 0.67                     | 1.05         | 0.81                     | 1.65          | 0.82                     | 1.14   | 1.60   |
| Y16 | 45.2  | 74.5  | 9.19 | 32.5  | 5.45 | 1.08 | 4.78 | 0.7  | 3.76 | 0.77 | 2.28 | 0.32 | 2.16 | 0.31 | 183.0        | 11.1 | 0.63                     | 0.99         | 0.85                     | 1.97          | 0.70                     | 0.27   | 2.42   |
| Y17 | 31.2  | 52.4  | 6.89 | 25.6  | 4.6  | 0.96 | 4.13 | 0.63 | 3.51 | 0.71 | 2.03 | 0.29 | 1.86 | 0.27 | 135.1        | 9.1  | 0.66                     | 1.03         | 0.84                     | 1.58          | 0.78                     | 0.71   | 1.64   |
| Y18 | 37.9  | 63.1  | 8.23 | 30.8  | 5.26 | 1.1  | 4.89 | 0.72 | 4.02 | 0.78 | 2.27 | 0.32 | 2.11 | 0.3  | 161.8        | 9.5  | 0.65                     | 1.01         | 0.84                     | 1.69          | 0.78                     | 0.44   | 1.83   |
| Y19 | 37.1  | 62.4  | 8.2  | 30.4  | 5.45 | 1.13 | 4.96 | 0.76 | 4.08 | 0.8  | 2.37 | 0.32 | 2.16 | 0.31 | 160.4        | 9.2  | 0.65                     | 1.01         | 0.84                     | 1.62          | 0.76                     | 0.46   | 1.77   |
| Y20 | 40.1  | 68.3  | 8.87 | 32.7  | 5.78 | 1.2  | 5.24 | 0.78 | 4.3  | 0.83 | 2.5  | 0.35 | 2.24 | 0.32 | 173.5        | 9.5  | 0.65                     | 1.02         | 0.85                     | 1.69          | 0.76                     | 0.35   | 1.80   |
| Y21 | 37.6  | 63.9  | 8.3  | 30.4  | 5.43 | 1.08 | 4.84 | 0.74 | 4.2  | 0.83 | 2.35 | 0.34 | 2.23 | 0.31 | 162.6        | 9.3  | 0.63                     | 0.98         | 0.85                     | 1.59          | 0.79                     | 0.44   | 1.75   |
| Y22 | 39.9  | 65.3  | 8.1  | 29.1  | 4.72 | 0.93 | 4.24 | 0.63 | 3.53 | 0.7  | 2.01 | 0.29 | 1.92 | 0.27 | 161.6        | 10.9 | 0.62                     | 0.97         | 0.84                     | 1.96          | 0.76                     | 0.44   | 2.23   |
| Y23 | 35.8  | 60.6  | 7.96 | 29.9  | 5.25 | 1.06 | 4.79 | 0.71 | 3.87 | 0.77 | 2.24 | 0.31 | 2.04 | 0.28 | 155.6        | 9.4  | 0.63                     | 0.98         | 0.84                     | 1.65          | 0.75                     | 0.51   | 1.80   |
| Y24 | 41.3  | 67.5  | 8.45 | 30.8  | 5.12 | 1.05 | 4.73 | 0.7  | 3.99 | 0.79 | 2.37 | 0.34 | 2.16 | 0.32 | 169.6        | 10.0 | 0.64                     | 0.99         | 0.84                     | 1.80          | 0.79                     | 0.36   | 1.95   |
| 均值  | 30.16 | 50.74 | 6.66 | 25.01 | 4.49 | 0.92 | 4.12 | 0.62 | 3.43 | 0.67 | 1.95 | 0.27 | 1.76 | 0.25 | 131.06       | 8.98 | 0.64                     | 1.00         | 0.84                     | 1.60          | 0.78                     | 0.84   | 1.63   |

注:L/R=LREE/HREE,LREE=La+Ce+Pr+Nd+Sm+Eu,HREE=Gd+Tb+Dy+Ho+Er+Tm+Yb+Lu; $\delta\text{Eu}_N=\frac{2w(\text{Eu})_N}{w(\text{Sm})_N+w(\text{Gd})_N}$ , $S=\text{PAAS}$ 标准化值(Taylor et al., 1985)。

$\delta\text{Eu}_S=\frac{2w(\text{Eu})_S}{w(\text{Sm})_S+w(\text{Gd})_S}$ , $\delta\text{Ce}_S=\frac{2w(\text{Ce})_S}{w(\text{La})_S+w(\text{Pr})_S}$ , $S$ 为PAAS标准化值(Haskin et al., 1968);

作用强弱判定指标(Cox et al., 1995; Bai Yueyue et al., 2015)。一般来说,成岩作用越强,则  $\delta\text{Ce}_s$  与  $\delta\text{Eu}_s$ 、 $\Sigma\text{REE}$ 、 $\text{Dy}_s/\text{Sm}_s$  相关性越好(张建军等,2017; 张茜等,2018a)。如图 3a、b、c 所示,研究区样品均呈现较差的相关性,指示成岩作用对元素的影响较弱。 $\text{Al}_2\text{O}_3-(\text{CaO}^*+\text{Na}_2\text{O})-\text{K}_2\text{O}$  图解(A—CN—K 图解)可用于判别碎屑岩风化作用、交代作用和物源组成(Fedo et al., 1995; Sensarma et al., 2008)。理想条件下,风化作用将沿着平行 A—CN 或 A—K 方向进行(牟传龙等,2019)(图 3d),交代作用使实际风化线与自然风化线偏离,偏离越大说明交代作用越强烈。在 A—CN—K 图解中研究区样品分布集中,且大部分沿 A—K 方向分布,实际风化线与自然风化线基本平行,说明样品在沉积期后交代作用微弱说明研究区龙马溪组泥岩元素地球化学特征受

后期成岩作用影响较小,可用于物源及风化作用的研究。

源岩属性是影响沉积岩化学组成的重要因素(Verma et al., 2017)。研究表明,中酸性岩具有较高的  $\text{K}_2\text{O}$ 、 $\text{Rb}$ 、 $\text{Al}_2\text{O}_3/\text{TiO}_2$  值和较低的  $\text{TiO}_2/\text{Zr}$  值(Floyd et al., 1989; Hayashi et al., 1997; Moradi et al., 2016)。研究区  $\text{K}_2\text{O}$  均值为 3.29% (表 2), 高于地壳均值(1.81%),也略高于上地壳均值(2.8%; Rudnick et al., 2004)。 $\text{Rb}$  均值为 104.5(表 3), 远高于地壳均值( $49 \times 10^{-6}$ )及上地壳均值( $82 \times 10^{-6}$ ; Rudnick et al., 2004)。同时,在  $\text{K}_2\text{O}-\text{Rb}$  图解中(图 4a),样品均落入中酸性成分区且数据集中,说明源岩为中酸性岩。研究区  $\text{Al}_2\text{O}_3/\text{TiO}_2$  较高,值为 21.68~34.34,远高于铁镁质火成岩(14),大多数落入长英质火成岩范围(18~26; Moradi et al., 2016;

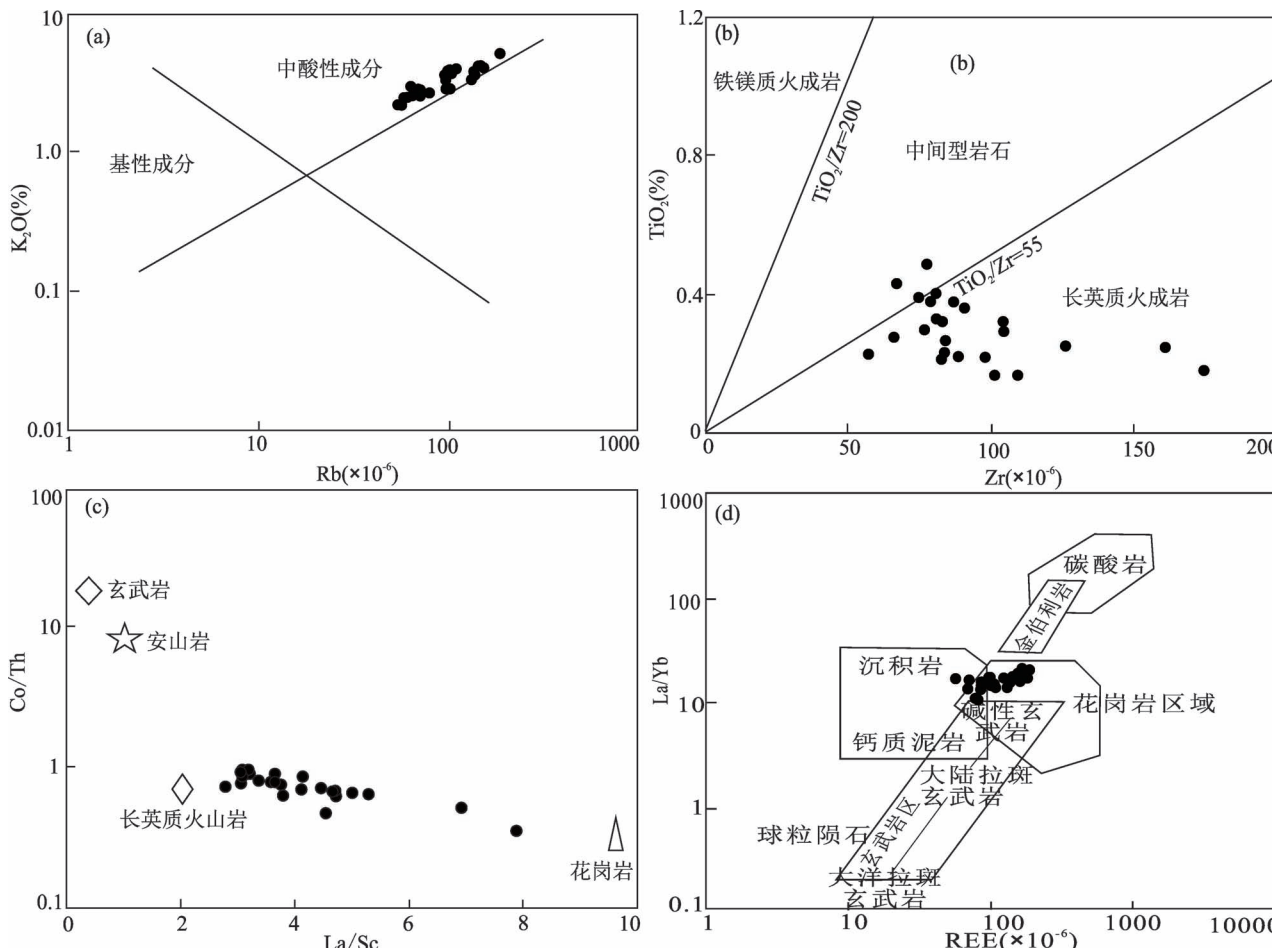


图 6 四川盆地清溪剖面源岩属性判别图解: (a)  $\text{K}_2\text{O}-\text{Rb}$  (据 Taylor and McLennan, 1985); (b)  $\text{Zr}-\text{TiO}_2$  (据 Hayashi et al., 1997); (c)  $\text{Co/Th}-\text{La/Sc}$  (据 Wang Zhongwei, 2018); (d)  $\text{La/Yb}-\Sigma\text{REE}$  (据 Allegre et al., 1974)

Fig. 6 Source rock properties discrimination diagrams of the Qingxi outcrop in the Sichuan Basin: (a)  $\text{K}_2\text{O}-\text{Rb}$  (after Taylor and McLennan, 1985); (b)  $\text{Zr}-\text{TiO}_2$  (after Hayashi et al., 1997); (c)  $\text{Co/Th}-\text{La/Sc}$  (after Wang Zhongwei, 2018); (d)  $\text{La/Yb}-\Sigma\text{REE}$  (after Allegre et al., 1974)

张建军等, 2017)。 $\text{TiO}_2/\text{Zr}$  值较低, 平均值为 34.76, 反应了长英质火成岩特征(<55; Hayashi et al., 1997)。同时, 在  $\text{TiO}_2-\text{Zr}$ (图 4b)二元图解中(Hayashi et al., 1997), 大多数样品落入长英质火成岩区, 少数样品点落入中间型岩石区, 说明源岩主要为偏酸性的长英质岩类。

随着岩浆的持续演化 La、Th 等微量元素富集, Sc、Cr、Co 等元素逐渐亏损, 因此, 酸性岩比基性岩有更高的 La/Sc 值、更低的 Co/Th 值(McLennan and Taylor, 1991; Wang Zhongwei, 2018)。研究区龙马溪组泥岩 La/Sc 较高, 均值为 4.11, Co/Th 较低, 均值为 0.73。在 Co/Th—La/Sc 图解(图 4c)中样品大多落入长英质火山岩及花岗岩之间的区域(Wang Zhongwei, 2018), 指示其母岩要主要为酸性的长英质岩类及花岗岩类。

稀土元素也可作为判定物源的参数, 通常中性斜长岩以  $\delta\text{Eu}_s$  正异常( $1.01 < \delta\text{Eu}_s < 2.33$ )为特征, 玄武岩以  $\delta\text{Eu}_s$  无异常( $0.90 < \delta\text{Eu}_s < 1.0$ ), 而酸性花岗岩多  $\delta\text{Eu}_s$  为负异常( $\delta\text{Eu}_s < 0.90$ )(张金亮等, 2007)。研究区龙马溪组样品的  $\delta\text{Eu}$  值为 0.60~0.67(表 4), 均值为 0.64, 明显负异常, 说明其源岩主要为酸性花岗岩。在  $\text{La}/\text{Yb}-\Sigma\text{REE}$  图解(图 4d)(Allegre et al., 1974; 周圆圆等, 2016), 样品点大部分落入花岗岩区域, 说明母岩主要古老沉积岩及花岗岩类等酸性岩类, 这与主量元素、微量元素的结论相符合。

综上, 通过主量、微量及稀土元素特综合判别可以得出研究区母岩主要为中酸性成分的岩类, 主要为长英质火成岩, 花岗岩等, 此类物源区可能为古老的地质体、克拉通或是再旋回造山带(Moradi et al., 2016; 张建军等, 2017)。

#### 4.2 物源风化作用

碎屑沉积岩  $\text{SiO}_2$  主要来自于石英碎屑,  $\text{Al}_2\text{O}_3$  主要来自于黏土矿物和长石, 因此,  $\text{SiO}_2$  含量及  $\text{SiO}_2/\text{Al}_2\text{O}_3$  用来反应沉积物的成熟度, 随着石英含量增多, 长石和基性矿物减少,  $\text{SiO}_2/\text{Al}_2\text{O}_3$  值增大, 沉积物成熟度升高(Roser et al., 1999)。样品  $\text{SiO}_2$  含量较低, 均值为 34% (表 2),  $\text{SiO}_2/\text{Al}_2\text{O}_3$  值较低, 平均值为 4.44, 说明清溪剖面龙马溪组泥岩成熟度较低, 不稳定成分的含量较高, 应为近源快速沉积的产物(张建军等, 2017)。

成分变异指数  $ICV = [n(\text{Fe}_2\text{O}_3) + n(\text{K}_2\text{O}^*) + n(\text{Na}_2\text{O}) + n(\text{CaO}^*) + n(\text{MgO}) + n(\text{MnO}) + n(\text{TiO}_2)] / n(\text{Al}_2\text{O}_3)$  用来判断碎屑沉积岩是初次

沉积还是再循环沉积(Cox et al., 1995), 其中  $\text{CaO}^*$  代表硅酸盐中的 CaO(全岩中的 CaO 去掉化学沉积的 CaO), 用  $\text{P}_2\text{O}_5$  的值来修正,  $n(\text{CaO}^*) = n(\text{CaO}) - n(\text{P}_2\text{O}_5)^* \times 10/3$ , 若修正后  $n(\text{CaO}^*)$  小于  $n(\text{Na}_2\text{O})$ , 那么 CaO 的值采用  $n(\text{CaO}^*)$ , 否则 CaO 的值假定等同于  $\text{Na}_2\text{O}$  (Wang Zhongwei, 2017)。 $\text{K}_2\text{O}^*$  代表消除 K 交代作用后的  $\text{K}_2\text{O}$  值, 在前面的分析中(图 3d)研究区样品受后期交代作用较小, 因此本文中  $\text{K}_2\text{O}^* = \text{K}_2\text{O}$  (Wang Zhongwei, 2017; 牟传龙等, 2019)。ICV 值低(<1)的碎屑沉积岩一般来自含有大量黏土矿物的沉积源区, 指示活动构造环境下沉积物的再循环或者较强风化条件下沉积物的初次沉积, 受后生作用的影响较大; 相反, ICV 值高(>1)的碎屑沉积岩则指示活动构造环境下的初次沉积(Van and Elgey, 1985)。研究区龙马溪组砂质泥岩 ICV 值为 0.80~6.35, 平均值为 2.13(表 2), 表明岩石中黏土矿物含量较低, 表明样品成分成熟度低, 源岩为首次沉积的沉积物, 并未受到再沉积作用的影响。

风化作用过程中 U 元素相对 Th 元素更活泼, 因此  $\text{Th}/\text{U}$  值随着化学风化程度增大而增加(Taylor and McLennan, 1985; 崔加伟等, 2016)。样品  $\text{Th}/\text{U}$  平均值为 3.92, 与地壳 UCC 值(3.8; Taylor and McLennan, 1985)相差不大, 说明物源区化学风化程度较弱。化学蚀变指数(chemical index of alteration, CIA)最初由 Nesbitt 和 Young (1982)提出用于判断物源区的化学风化作用强度,  $CIA = 100 \times n(\text{Al}_2\text{O}_3) / [(n(\text{Al}_2\text{O}_3) + n(\text{CaO}^*) + n(\text{Na}_2\text{O}) + n(\text{K}_2\text{O})]$ ,  $\text{CaO}^*$  计算方式同上。在化学风化作用过程中, 不稳定矿物如长石及暗色矿物的  $\text{Ca}^{2+}$ 、 $\text{Na}^+$ 、 $\text{K}^+$  等随地表流体大量流失, 而稳定矿物的  $\text{Al}^{3+}$ 、 $\text{Ti}^{4+}$  等残留保存, 因此 CIA 值随着风化作用增强而增大。随着研究的不断深入, CIA 值也用于指示沉积期古气候环境(Nesbitt and Young, 1984, 1989)。普遍认为  $CIA = 85 \sim 100$  代表炎热、潮湿环境下的强烈风化作用,  $CIA = 65 \sim 85$  指示温暖、湿润环境下的中等风化,  $CIA = 50 \sim 65$  反映寒冷、干燥环境下的初级风化作用。通常情况下, 物源区母岩物质是复杂的, 用 CIA 进行定量分析物源区古风化作用强度及古气候时, 还应考虑到沉积分异作用、再旋回作用、沉积区进一步风化作用以及成岩期钾质交代等作用的影响。上面提到清溪剖面龙马溪组样品 ICV 值大于 1 表明该区未受到再旋回作用的影响, 且受到钾质交代的影响也较弱。研究区样品 CIA 值为 55~71, 均值为 64, 说明物源区

整体受风化程度较低,气候较为寒冷、干燥。其中龙马溪组下部样品的 CIA 值为 55~63,均值为 60(图 4,表 2),指示寒冷、干燥环境下的初级风化作用。上部样品 CIA 值有上升的趋势,值为 58~71,均值为 68,温暖、湿润环境下的中等风化。表明龙马溪组从早期到晚期古风化作用强度增大,气候变暖。

同样的,研究表明高的 Rb/Sr 值指示温暖、潮湿环境,低的 Rb/Sr 值指示干燥、寒冷环境(罗情勇等,2013)。研究区 Rb/Sr 值较小,为 0.22~1.06,均值为 0.51,低于澳大利亚后太古宙平均页岩(约 0.8)(Taylor and McLennan, 1985),说明其沉积气候干燥寒冷,与前面得出的结论一致。研究认为,由于构造活动强烈,初次沉积物接受风化作用的时间较短,难以被强烈风化。而经历多次旋回沉积的沉积物,多次接受风化作用所以风化程度较强,这与本文所得结论一致。综合以上分析表明,研究区龙马溪组泥岩物源为活动构造环境下初次旋回的快速沉积产物,受到的化学风化强度较弱,沉积期环境总体干燥、寒冷。

#### 4.3 构造背景

在沉积建造中,陆源碎屑岩的地球化学特征不仅保留着物源区源岩的相关信息,也在一定程度上记录了沉积过程中构造活动变化情况,常用于推断沉积盆地的构造演化历史(Bauluz et al., 2000)。稀土元素及一些惰性元素如 Sc、Zr、Ti、Th 等在沉积成岩作用中稳定性较好,常用于物源区属性和大地构造背景研究(Bhatia, 1985; Bhatia and Crook, 1986)。一般来说,处于被动大陆边缘的沉积物的稀土元素特征与与太古宙之后页岩的稀土元素相似,以轻稀土富集,Eu 负异常为特点;处于活动大陆边缘的沉积物母岩主要为分异程度较低的火山岩,以重稀土富集,无 Eu 亏损为特征(赵振华,1978)。研究区稀土元素总量  $\Sigma\text{REE}$  为  $53.2 \times 10^{-6} \sim 183 \times 10^{-6}$ ,均值为  $131.1 \times 10^{-6}$ ,与页岩的稀土元素平均值(范德廉等,1987)接近, $\Sigma\text{LREE}/\Sigma\text{HREE}$  平均值为  $8.98 \times 10^{-6}$ ,轻稀土明显富集, $\delta\text{Eu}_N$  平均值为 0.64,显示负异常,指示构造背景为被动大陆边缘。同时,La/Yb、(La<sub>N</sub>/Yb<sub>N</sub>)、LREE/HREE、La 以及 Sc/Cr 值全部表现出与被动大陆边缘相近的特征(表 5)。同时在构造背景相关图解中,如 Sc/Cr—La/Y 图解(Roser and Korsch, 1986)(图 7)及 La—Sc—Th 判别图(图 8a)(Bhatia and Crook, 1986)

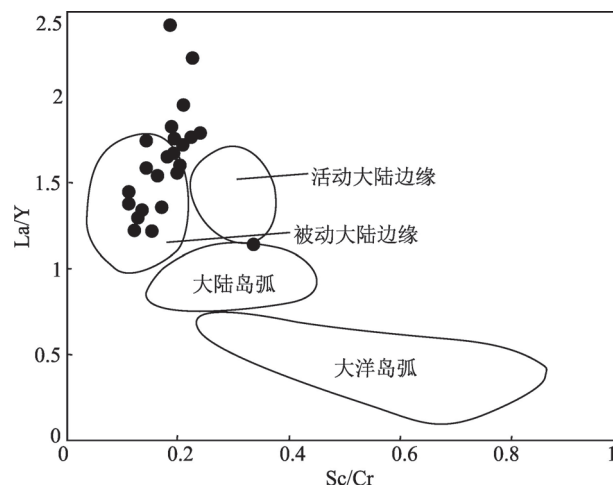


图 7 四川盆地清溪剖面龙马溪组 La/Y—Sc/Cr 判别图  
(底图据 Roser and Korsch, 1986)

Fig. 7 Discrimination diagrams of La /Y—Sc /Cr of Qingxi outcrop in the Sichuan Basin ( Base map from Roser and Korsch, 1986)

ACM—活动大陆边缘; PM—被动大陆边缘; CIA—大陆岛弧;  
OIA—大洋岛弧

ACM—active continental margin; PM—passive continental margin;  
CIA—continental island arc; OIA—oceanic island arc

样品投点较为集中,大多数落入被动大陆边缘及其附近区域,而在 Th—Co—Zr/10(图 8b)、Th—Sc—Zr/10(图 8c; Bhatia and Crook, 1986) 样品点分布较为分散,部分落在被动大陆边缘,部分落入活动大陆边缘及大陆岛弧以及以外的区域,识别出的较为复杂的构造背景,这有可能与构图微量元素活性较强所以识图能力较弱相关(Verma and Armstrong-Altrin, 2013; Tawfik et al., 2015)。加之前人在研究物源区构造背景时发现,以被动大陆边缘为主要物源的岩石中通常包含较多的活动大陆边缘和/或大陆岛弧的地球化学信息(柏道远等,2007; 田洋等,2015)。因此本文基于岩石地球化学特征结合区

表 5 四川盆地清溪剖面构造背景对比表

Table 5 Tectonic background comparison of the Qingxi outcrop  
in the Sichuan Basin

| 构造环境                 | 大洋岛弧            | 大陆岛弧            | 活动大陆边缘          | 被动大陆边缘          | 本文平均值 |
|----------------------|-----------------|-----------------|-----------------|-----------------|-------|
| La                   | $8.72 \pm 2.5$  | $24.4 \pm 2.3$  | $33 \pm 4.5$    | $33.5 \pm 5.8$  | 33.16 |
| Sc/Cr                | $0.57 \pm 0.16$ | $0.32 \pm 0.06$ | $0.30 \pm 0.02$ | $0.16 \pm 0.02$ | 0.18  |
| LREE/HREE            | $3.8 \pm 0.9$   | $7.7 \pm 1.7$   | 9.1             | 8.5             | 8.98  |
| La/Yb                | $4.2 \pm 1.3$   | $11.0 \pm 3.6$  | 12.5            | 15.9            | 16.95 |
| (La/Yb) <sub>N</sub> | $2.8 \pm 0.9$   | $7.5 \pm 2.5$   | 8.5             | 10.8            | 9.85  |

资料来源:Bhatia, 1985; Bhatia and Crook, 1986。

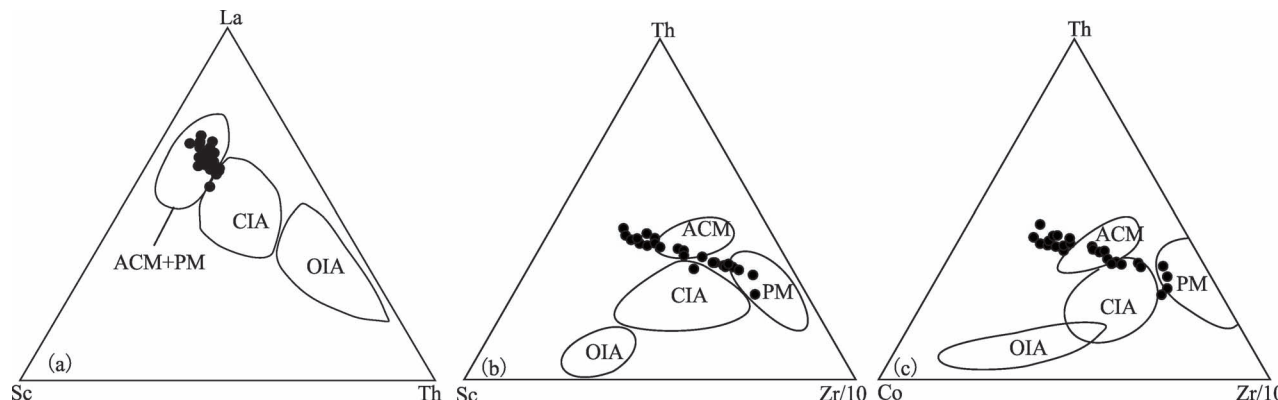


图8 四川盆地清溪剖面构造背景判别图解(底图据 Bhatia and Crook, 1986)

Fig. 8 Diagrams for tectonic setting of Qingxi outcrop in the Sichuan Basin (Base map from Bhatia and Crook 1986)

ACM—活动大陆边缘; PM—被动大陆边缘; CIA—大陆岛弧; OIA—大洋岛弧

ACM—active continental margin; PM—passive continental margin; CIA—continental island arc; OIA—oceanic island arc

域地质背景得出龙马溪组沉积构造背景为被动大陆边缘。

#### 4.4 地质意义

扬子地台西南缘构造复杂,大致可概括为中元古代褶皱基底形成后,继而转化为新元古代早期—三叠纪被动大陆边缘环境,以后卷入中生代碰撞造山过程,最终在新生代发生陆内造山作用(骆耀南,1983;梅庆华等,2016)。在奥陶纪—志留纪之交,随着华南板块持续向北俯冲并与滇缅、华北等板块碰撞和拼合,扬子地台发生板内变形自东南缘向西北逐次向下挠曲并形成深水前陆盆地,建造了五峰组—龙马溪组黑色页岩(樊隽轩等,2012;牟传龙等,2015)。除扬子板块北缘仍处在被动大陆边缘外,其他地区均表现出挤压收缩的构造背景(梅冥相等,2005)。扬子西缘康滇古陆与川中隆起之间为一深水海槽与外海相连,通过地质调查发现,该海槽区域沉积的龙马溪组钙质砂质明显较盆内高,白云质发育,推测该区可能局部因碰撞挤压形成了介于两大隆起鞍部的小型水下高地或者隆起,使得该区龙马溪组沉积期相变较大。但扬子西缘整体处于持续抬升状态,仍属被动大陆边缘环境(陈旭等,2014;聂海宽等,2017),这与本文基于地球化学特征得出构造背景相一致。晚奥陶世—早志留世这一特殊时期全球范围内也发生了多个大事件,晚奥陶世赫南特期的生物大灭绝事件,同时期冈瓦纳大陆冰川事件波及全球,赫南特期存在短暂时间的冰期(Chen Xu et al., 2004; 李双建等,2008),沉积了观音桥段介壳灰岩,荣经地区也有该沉积响应。然后气候回暖,冰雪消融,海平面上涨,使得底层水体滞

留还原沉积了深水陆棚相龙马溪组富有机质页岩。而扬子西缘受构造隆升影响,研究区龙马溪期水体较浅,呈现弱还原环境。但是依然继承了奥陶纪晚期全球寒冷干旱的古气候,经历了低等化学风化作用。

研究区西侧的康滇古陆属扬子地台西南缘二级构造单元,是显生宙以来长期出露的地区(刘家铎等,2004)。前寒武纪以前,是康滇古陆的岛弧褶皱带形成期,晋宁运动使得康滇弧系褶皱成山而转换成了早震旦世的安弟斯型山弧,并与扬子大陆结成统一的扬子板块大陆。晚震旦世开始,康滇构造带进入板内稳定地台发展阶段,中奥陶以后,由于地幔物质上涌,上地壳发生成穹作用,出现大面积的构造隆升然后成穹,一直持续到二叠纪。研究发现,荣经地区邻近的古陆地区,如沪定—石绵一线主要出露新元古代地台盖层,岩性为典型钙碱系列的中酸性火山岩—火山碎屑岩系,并伴以同源花岗岩类的大量侵位(骆耀南,1983; 刘家铎等,2004)。而康定—沪定地区,主要出露太古宙结晶基底,由“康定杂岩”组成,岩性主要为角闪岩相—磨拉岩相的斜长花岗片麻岩及石英闪长片麻岩伴以层状超镁铁—镁铁质岩残留体(骆耀南,1983; 刘家铎等,2004)。本文岩石学、矿物学及地球化学特征指示研究区母岩为中酸性岩类,主要为长英质火成岩,花岗岩类,推测其母岩主要由康滇古陆新元古早期地台盖层提供。研究区东侧的川中隆起经历了多期的构造升降运动,在加里东晚期整体抬升,遭受剥蚀,一直持续到二叠系沉积之前。但在志留纪早期,川中隆起是否出露地表接受沉积或是为水下降起,目前尚未有

定论(梅庆华等, 2016; 周恩恩等, 2016; 王玉满等, 2017)。加之本项目团队在野外地质调查中并未在川中隆起周缘看见潮坪相沉积(图 1a), 因此本文认为荣经地区龙马溪期源岩主要由康滇古陆提供。

## 5 结论

通过对荣经地区龙马溪组泥质岩系的岩石学特征与地球化学特征系统研究表明:

(1) 荣经地区下志留统龙马溪组泥岩总体砂质、钙质含量较高, 偶见笔石及少量生物碎屑, 白云质含量较高。镜下可见草莓状黄铁矿, 偶见有机质。Mo、U、V、Ni 等元素弱富集, Cu、Zn 等元素亏损, 指示龙马溪期沉积水体还原性较弱, 古生产力较低, 沉积水体较浅。结合区域地质调查, 推测在川中隆起及康滇古陆之间的深水海槽内可能存在小型隆升或水下降起, 使得荣经地区龙马溪组沉积期相变较大。

(2)  $\delta\text{Ce}_s - \delta\text{Eu}_s$ 、 $\delta\text{Ce}_s - \Sigma\text{REE}$ 、 $\delta\text{Ce}_s - \text{Dy}_s/\text{Sm}_s$  以及 A—CN—K 图解说明荣经地区下志留统龙马溪组泥岩化学成分受后期成岩作用及交代作用影响较小, 可用于物源及其风化作用的研究。研究区龙马溪组泥岩  $\text{K}_2\text{O}$ 、Rb、 $\text{Al}_2\text{O}_3/\text{TiO}_2$  值较高,  $\delta\text{Eu}_N$  呈现明显负异常, 结合 Co/Th—La/Sc 图解、La/Yb— $\Sigma\text{REE}$  等图解综合说明母岩为中酸性成分的岩类, 主要为长英质火成岩, 花岗岩类, 此类物源区可能为古老的地质体、克拉通或是再旋回造山带。推测其母岩主要由西侧的康滇古陆新元古早期地台盖层提供。

(3) 研究区龙马溪组泥岩  $\text{SiO}_2/\text{Al}_2\text{O}_3$  较低, 指示其成熟度较低, 不稳定成分含量较高, 为近源快速沉积的产物。 $ICV$  值大于 1,  $CIA$  平均值为 66,  $\text{Th}/\text{U}$  为 3.92, 与地壳 UCC 值相近,  $\text{Rb}/\text{Sr}$  值较小, 明显低于 PAAS, 指示其物源为活动构造环境下初次旋回的快速沉积产物, 受化学风化作用较小, 沉积环境为干燥、寒冷环境。

(4) 研究区  $\delta\text{Eu}$  负异常, 轻稀土富集, La/Yb,  $(\text{La}/\text{Yb})_N$ 、LREE/HREE、La, 以及 Sc/Cr 等元素特征结合相关构造判别图解说明研究区沉积构造背景主要为被动大陆边缘。

**致谢:**感谢中国地质调查局成都地质调查中心冯心涛高工团队、葛祥英工程师团队和戴婕高工在野外工作中以及论文撰写过程中给予的帮助, 同时对审稿专家的严格审稿和建设性建议致以衷心感谢。

## 参 考 文 献 / References

- (The literature whose publishing year followed by a “&” is in Chinese with English abstract; The literature whose publishing year followed by a “#” is in Chinese without English abstract)
- 柏道远, 周亮, 王先辉, 张晓阳, 马铁球. 2007. 湘东南南华系—寒武系砂岩地球化学特征及对华南新元古代—早古生代构造背景的制约. 地质学报, 81(6): 755~771.
- 陈旭, 樊隽轩, 陈清, 唐兰, 侯旭东. 2014. 论广西运动的阶段性. 中国科学: 地球科学, 44(5): 842~850.
- 崔加伟, 郑有业, 孙祥, 田立明, 孙君一. 2016. 松潘—甘孜造山带北段岗龙乡花岗岩岩石成因及地球动力学特征. 地质科技情报, 35(2): 129~139.
- 杜远生, 朱杰, 顾松竹, 徐亚军, 杨江海. 2007. 北祁连造山带寒武系—奥陶系硅质岩沉积地球化学特征及其对多岛洋的启示. 中国科学: 地球科学, 37(10): 1314~1329.
- 范德廉, 叶杰, 杨瑞英, 黄忠祥. 1987. 扬子地台前寒武—寒武纪界线附近的地质事件与成矿作用. 沉积学报, 5(3): 81~95+181.
- 樊隽轩, Michael J M, 陈旭, 王怿, 张元动, 陈清, 迟昭利, 陈峰. 2012. 华南奥陶—志留系龙马溪组黑色笔石页岩的生物地层学. 中国科学: 地球科学, 42(1): 130~139.
- 冯动军, 胡宗全, 高波, 彭勇民, 杜伟. 2016. 川东南地区五峰组—龙马溪组页岩气成藏条件分析. 地质论评, 62(6): 1521~1532.
- 冯连君, 储雪蕾, 张启锐, 张同钢. 2003. 化学蚀变指数 (CIA) 及其在新元古代碎屑岩中的应用. 地学前缘, 10(4): 539~544.
- 冯仁蔚, 王兴志, 张帆, 庞艳君. 2008. 川西南周公山及邻区下二叠统碳酸盐岩成岩作用对储集性的影响. 地质找矿论丛, 23(3): 223~229.
- 巩磊, 王超勇, 杨永国, 周豪. 2014. 川西南与川东北地区下志留统龙马溪组页岩气成藏条件对比及目标区分析. 地质科技情报, 33(5): 128~133.
- 何登发, 李德生, 张国伟, 赵路子, 樊春, 鲁人齐, 文竹. 2011. 四川多旋回叠合盆地的形成与演化. 地质科学, 46(3): 589~606.
- 李伟, 易海永, 胡望水, 杨庚, 熊璇. 2014. 四川盆地加里东古隆起构造演化与油气聚集的关系. 天然气工业, 34(3): 8~15.
- 李双建, 肖开华, 沃玉进, 龙胜祥, 蔡立国. 2008. 南方海相上奥陶统一下志留统优质烃源岩发育的控制因素. 沉积学报, 26(5): 872~882.
- 李艳芳, 邵德勇, 吕海刚, 张瑜. 2015. 四川盆地五峰组—龙马溪组海相页岩元素地球化学特征与有机质富集的关系. 石油学报, 36(12): 1470~1482.
- 刘家铎, 张成江, 刘显凡, 李佑国, 阳正熙, 吴德超. 2004. 扬子地台西南缘成矿规律及找矿方向. 北京: 地质出版社.
- 罗情勇, 钟宁宁, 朱雷, 王延年, 秦婧, 齐琳, 张毅, 马勇. 2013. 华北北部中元古界洪水庄组埋藏有机碳与古生产力的相关性. 科学通报, 58(11): 1036~1047.
- 骆耀南. 1983. 康滇构造带的古板块历史演化. 地球科学, 3(22): 93~101.
- 梅冥相, 马永生, 邓军, 李浩, 郑宽兵. 2005. 加里东运动构造古地理及滇黔桂盆地的形成——兼论滇黔桂盆地深层油气勘探潜力. 地学前缘, 12(3): 227~236.
- 梅庆华, 何登发, 宝玲, 李英强, 赖李, 李传新. 2016. 川中地区新元古代—古生代初多幕裂陷过程及其演化. 天然气地球科学, 27(8): 1427~1438.
- 牟传龙, 葛祥英, 周恩恩, 王秀平. 2015. 川西南晚奥陶世五峰期岩

- 相古地理. 中国地质, 42(1): 192~198.
- 牟传龙, 王秀平, 王启宇, 周恩恩, 梁薇, 葛祥英, 陈小炜. 2016. 川南及邻区下志留统龙马溪组下段沉积相与页岩气地质条件的关系. 古地理学报, 18(3): 457~472.
- 牟传龙, 葛祥英, 余谦, 门欣, 刘伟, 何江林, 梁薇. 2019. 川西南地区五峰—龙马溪组黑色页岩古气候及物源特征: 来自新地2井地球化学记录. 古地理学报, 21(5): 835~846.
- 聂海宽, 金之钧, 边瑞康, 杜伟. 2016. 四川盆地及其周缘上奥陶统五峰组一下志留统龙马溪组页岩气“源—盖控藏”富集. 石油学报, 37(5): 557~571.
- 聂海宽, 金之钧, 马鑫, 刘忠宝, 林拓, 杨振恒. 2017. 四川盆地及邻区上奥陶统五峰组一下志留统龙马溪组底部笔石带及沉积特征. 石油学报, 38(2): 160~174.
- 蒲泊伶, 董大忠, 王凤琴, 王玉满, 黄金亮. 2020. 沉积相带对川南龙马溪组页岩气富集的影响. 中国地质, 47(1): 111~120.
- 任军平, 左立波, 许康康, 王杰, 刘晓阳, 何胜飞, 刘宇, 贺福清. 2016. 赞比亚北部班韦卢地块演化及矿产资源研究. 地质论评, 62(4): 979~996.
- 田洋, 赵小明, 王令占, 涂兵, 谢国刚, 曾波夫. 2015. 鄂西南利川三叠纪须家河组地球化学特征及其对风化、物源与构造背景的指示. 岩石学报, 31(1): 261~272.
- 王启宇, 牟传龙, 贺娟, 同国川, 凌亚军, 孙小勇. 2018. 维西地区中三叠统上兰组物源分析及构造背景判断. 地球科学, 43(8): 2811~2832.
- 王玉满, 董大忠, 黄金亮, 李新景, 王淑芳. 2016. 四川盆地及周边上奥陶统五峰组观音桥段岩相特征及对页岩气选区意义. 石油勘探与开发, 43(1): 42~50.
- 王玉满, 李新景, 董大忠, 张晨晨, 王淑芳. 2017. 上扬子地区五峰组—龙马溪组优质页岩沉积主控因素. 天然气工业, 37(4): 9~20.
- 吴安彬, 张景坤, 王井伶, 罗家国, 罗群, 姜振学. 2020. 富有机质页岩方解石脉成因、成岩模式与地质意义——以四川盆地南部龙马溪组为例. 地质论评, 66(1): 88~99.
- 吴蓝宇, 胡东风, 陆永潮, 刘若冰, 刘晓峰. 2016. 四川盆地涪陵气田五峰组—龙马溪组页岩优势岩相. 石油勘探与开发, 43(2): 189~197.
- 严德天, 王清晨, 陈代钊, 汪建国, 王卓卓. 2008. 扬子及周缘地区上奥陶统一下志留统烃源岩发育环境及其控制因素. 地质学报, 82(3): 321~327.
- 余谦, 牟传龙, 张海全, 谭钦银. 2011. 上扬子北缘震旦纪—早古生代沉积演化与储层分布特征. 岩石学报, 27(3): 672~680.
- 袁桃, 魏祥峰, 张汉荣, 李春燕, 魏富彬, 卢龙飞, 王强. 2020. 四川盆地及周缘上奥陶统五峰组一下志留统龙马溪组页岩岩相划分. 石油实验地质, 42(3): 371~381.
- 张建军, 牟传龙, 周恩恩, 冯丽霞, 伍皓, 陈小炜. 2017. 滇西户撒盆地芒棒组砂岩地球化学特征及物源区和构造背景分析. 地质学报, 91(5): 1083~1096.
- 张金亮, 张鑫. 2007. 塔中地区志留系砂岩元素地球化学特征与物源判别意义. 岩石学报, 23(11): 2990~3002.
- 张茜, 王剑, 余谦, 王小飞, 赵安坤, 雷子慧. 2016. 川西南构造复杂区龙马溪组地球化学特征及古环境. 新疆石油地质, 38(4): 399~406.
- 张茜, 余谦, 王剑, 肖渊甫, 程锦翔, 赵安坤, 张彬. 2018a. 应用ICP—MS研究川西南龙马溪组泥页岩稀土元素特征及沉积环境. 岩矿测试, 37(2): 217~224.
- 张茜, 王剑, 余谦, 肖渊甫, 张彬, 王晓飞, 赵安坤. 2018b. 扬子地台西缘盐源盆地下志留统龙马溪组黑色页岩硅质成因及沉积环境. 地质论评, 64(3): 610~622.
- 赵振华. 1978. 稀土元素地球化学特征及其在岩石和矿床成因研究中的应用. 地球与环境, 33(9): 3~13.
- 郑志红, 李登华, 白森舒, 贾君, 胥昕, 刘卓亚, 高熹. 2017. 四川盆地天然气资源潜力. 中国石油勘探, 22(3): 12~20.
- 周圆圆, 邱楠生, 腾格尔, 王杰, 曹涛涛, 罗厚勇. 2016. 茂名油柑窝组油页岩元素地球化学特征及其地质意义. 矿物岩石地球化学通报, 35(6): 1270~1279.
- 周恩恩, 许效松. 2016. 扬子陆块西部古隆起演化及其对郁南运动的反映. 地质论评, 62(5): 1125~1133.
- 钟勇, 李亚林, 张晓斌, 刘树根, 巫芙蓉, 刘定锦, 邓小江, 陈胜, 杨飞, 李小娟, 蒋波. 2014. 川中古隆起构造演化特征及其与早寒武世绵阳—长宁拉张槽的关系. 成都理工大学学报(自然科学版), 45(6): 703~712.
- Algeo T J, Tribouillard N. 2009. Environmental analysis of paleoceanographic systems based on molybdenum – uranium covariation. Chemical Geology, 268(3~4): 211~225.
- Allegre C J, Birck J L, Loubet M. 1974. Provost. A Rb–Sr age and content of potassium, rubidium strontium, barium, and rare earths in surface material from the Sea of Fertility. In: Lunar Soil from the Sea of Fertility: 436~440.
- Andersen T. 2005. Detrital zircons as tracers of sedimentary provenance: limiting conditions from statistics and numerical simulation. Chemical Geology, 216(3): 249~270.
- Bai Daoyuan, Zhou Liang, Wang Xianhui, Zhang Xiaoyang, Ma Tieqiu. 2007&. Geochemistry of Nanhuan – Cambrian sandstones in southeastern Hunan, and its constraints on Neoproterozoic – Early Paleozoic tectonic setting of South China. Acta Geologica sinica, 81(6): 755~771.
- Bai Yueyue, Liu Zhaojun, Sun Pingchang, Liu Rong, Hu Xiaofeng, Zhao Hanqing, Xu Yinbo. 2015. Rare earth and major element geochemistry of Eocene fine-grained sediments in oil shale – and coal-bearing layers of the Meihé Basin, Northeast China. Journal of Asian Earth Sciences, 97: 89~101.
- Bauluz B, Mayayo M J, Fernandez – Nieto C, Lopez J M G. 2000. Geochemistry of Precambrian and Paleozoic siliciclastic rocks from the Iberian Range (NE Spain): implications for source – area weathering, sorting, provenance, and tectonic setting. Chemical Geology, 168(1): 135~150.
- Bhatia M R. 1985. Rare earth element geochemistry of Australian Paleozoic graywackes and mudrocks: Provenance and tectonic control. Sedimentary Geology, 45(1): 97~113.
- Bhatia M R, Crook K A. 1986. Trace element characteristics of greywackes and tectonic setting discrimination of sedimentary basins. Contributions to Mineralogy and Petrology, 92(2): 181~193.
- Chen Xu, Fan Junxuan, Chen Qing, Tang Lan, Hou Xudong. 2014&. Toward a stepwise Kwangshian Orogeny. Scientia Sinica, 44(5): 842~850.
- Chen Xu, Rong Jiayu, Li Yue, Boucot A J. 2004. Facies patterns and geography of the Yangtze region, South China, through the Ordovician and Silurian transition. Palaeogeography, Palaeoclimatology, Palaeoecology, 204(3~4): 353~372.
- Cui Jiawei, Zheng Youye, Sun Xiang, Tian Liming, Sun Junyi. 2016&. Petrogenesis and geodynamics characteristics of Ganglong in the north of Songpan – Ganzi fold belt. Geological Science and Technology Information, 35(2): 129~139.
- Cox R, Lowe D R, Cullers R L. 1995. The influence of sediment recycling and basement composition on evolution of mudrock chemistry in Southwestern United States. Geochimcosmochimacta,

- 59(14): 2919~2940.
- Dickinson W R. 1985. Interpreting Provenance Relations from Detrital Modes of Sandstones. D. Reidel Publishing Company: 335~361.
- Du Yuansheng, Zhu Jie, Gu Sunzhu, Xu Yajun, Yang Jianghai. 2007&. Sedimentary geochemical characteristics of Cambrian – ordovician siliceous rocks in the northern qilian orogenic belt and their implications for multi-island oceans. *Science in China (Series D: Earth Sciences)*, 37(10): 1314~1329.
- Fan Delian, Ye Jie, Yang Ruiying, Huang Zhongxiang. 1987&. The geological events and ore mineralization nearby the Precambrian – Cambrian boundary in Yangtze Platform. *Acta Sedimentologica Sinica*, 5(3): 81~95+181.
- Fan Junxuan, Michael J M, Chen Xu, Wang Yi, Zhang Yuandong, Chen Qing, Chi Zhaoli, Chen Feng. 2012&. Biostratigraphy of the black pencil stone shale of the Ordovician – Silurian Longmaxi Formation in South China. *Chinese Science: Earth Science*, 42(1): 130~139.
- Fedo C M, Nesbitt H W, Young G M. 1995. Unraveling the effects of potassium metasomatism in sedimentary rocks and paleosols, with implications for paleoweathering conditions and provenance. *Geology*, 23(10): 921~924.
- Feng Dongjun, Hu Zongquan, Gao Bo, Peng Yongmin, Du Wei. 2016. Analysis of shale gas reservoir-forming condition of Wufeng Formation —Longmaxi Formation in Southeast Sichuan Basin. *Geological Review*, 62(6): 1521~1532.
- Feng Lianjun, ChuXuelie, Zhang Qirui, Zhang Tonggang. 2003&. CIA (Chemical index of alteration) and its applications in the Neoproterozoic calcareous rocks. *Earth Science Frontiers*, 10(4): 539~544.
- Feng Renwei, Wang Xingzhi, Zhang Fan, Pang Yanjun. 2008&. Influence of diagenesis of lower permian carbonate on reservoir performance in Zhou gongshan and the near district in the southwest Sichuan. *Contributions to Geology and Mineral Resources Research*, 23(3): 223~229.
- Floyd P A, Winchester J A, Park R G. 1989. Geochemistry and tectonic setting of Lewisian clastic metasediments from the Early Proterozoic Loch Maree Group of Gairloch, NW Scotland. *Precambrian Research*, 45(1~3): 203~214.
- Gong Lei, Wang Chaoyong, Yang Yongguo, Zhou Hao. 2014&. Comparison of reservoir-forming conditions and objective exploration zones of shale gas in Lower Silurian Longmaxi Formation of southwest and northeast Sichuan Basin. *Geological Science and Technology Information*, 33(5): 128~133.
- Haskin L, Wildeman T, Haskin M. 1968. An accurate procedure for the determination of the rare earths by neutron activation. *Journal of Radioanalytical Chemistry*, 1(4): 337~348.
- Hayashi K I, Fujisawa H, Holland H D, Ohmoto H. 1997. Geochemistry of approximately 1.9 Ga sedimentary rocks from northeastern Labrador, Canada. *Geochimica et Cosmochimica Acta*, 61(19): 4115~4137.
- He Dengfa, Li Desheng, Zhang Guowei, Zhao Luzi, Fan Chun, Lu Renqi, Wen Zhu. 2011&. Formation and evolution of multi-cycle superposed Sichuan Basin. *China Chinese Journal of Geology*, 46(3): 589~606.
- Johnsson M J. 1993. The system controlling the composition of clastic sediments. *Geological Society of America Special Paper*, 284: 1~19.
- Li Wie, Yi Haiyong, Hu Wangshui, Yang Gen, Xiong Xuan. 2014&. Tectonic evolution of Caledonian paleohigh in the Sichuan basin and its relationship with hydrocarbon accumulation. *Natural Gas Industry*, 34(3): 8~15.
- Li Shuangjian, Xiao Kaihua, Wo Yujin, Long Shengxiang, Cai Liguo. 2008&. Developmental controlling factors of Upper Ordovician – Lower Silurian high quality source rocks in marine sequence, South China. *Acta Sedimentologica Sinica*, 26(5): 872~882.
- Li Yanfang, Zhang Tongwei, Geoffrey S. Ellis, Shao Deyong. 2017. Depositional environment and organic matter accumulation of Upper Ordovician – Lower Silurian marine shale in the Upper Yangtze Platform, South China. *Palaeogeography, Palaeoclimatology, Palaeoecology*, 466: 252~264.
- Li Yanfang, Shao Deyong, Lv Haigang, Zhang Yu, Zhang Xilong, Zhang Tongwei. 2015&. A relationship between elemental geochemical characteristics and organic matter enrichment in marine shale of Wufeng Formation – Longmaxi Formation, Sichuan Basin. *Acta Petrolei Sinica*, 36(12): 1470~1482.
- Liu Jiaduo, Zhang Chengjiang, Liu Xianfan, Li Youguo, Yang Zhengxi, Wu Dechao. 2004&. *The Metallogenetic Regularity and Prospecting Direction of the Southwestern Margin of Yangtze Platform*. Beijing: Geological Publishing House.
- Luo Qingyong, Zhong Ningning, Zhu Lei, Wang Yannian, Qin Jing, Qiling, Zhang Yi, Ma Yong. 2013&. Correlation of burial organic carbon and paleoproductivity in the Mesoproterozoic Hongshuihuang Formation, northern North China. *Chinese Science Bulletin*, 58(11): 1036~1047.
- Luo Yaonan. 1983&. The evolution of paleoplates in the Kang – Dian tectonic zone. *Earth Science*, 3(22): 93~101.
- Ma Yiquan, Fan Majie, Lu Yongchao, Guo Xusheng, Hu Haiyan, Chen Lei, Wang Chao, Liu Xiaochen. 2016. Geochemistry and sedimentology of the Lower Silurian Longmaxi mudstone in southwestern China: implications for depositional controls on organic matter accumulation. *Marine and Petroleum Geology*, 75: 291~309.
- McLennan S, Hemming S, McDaniel D, Hanson G. 1993. Geochemical approaches to sedimentation, provenance, and tectonics. *Geological Society of America Special Papers*, 284: 21~40.
- McLennan S M, Taylor S R. 1991. Sedimentary rocks and crustal evolution: tectonic setting and secular trends. *Journal of Geology*, 99(1): 1~21.
- Mei Mingxiang, Ma Yongsheng, Deng Jun, Li Hao, Zheng Kuanbin. 2005&. Tectonic palaeogeographic changes resulting from the Caledonian movement and the formation of the Dianqiangui Basin: Discussion on the deep exploration potential of oil and gas in the Dianqiangui Basin. *Earth Science Frontiers*, 12(3): 227~236.
- Mei Qinghua, He Dengfa, Gui Baoling, Li Yingqiang, Li Jiao, Li Chuanxin. 2016&. Multiple rifting and its evolution of central Sichuan Basin in the Neoproterozoic – Paleozoic. *Natural Gas Geoscience*, 27(8): 1427~1438.
- Moradi A V, Sari A, Akkaya P. 2016. Geochemistry of the Miocene oil shale (Hançılı Formation) in the Çankırı – Çorum Basin, Central Turkey: Implications for Paleoclimate conditions, source – area weathering, provenance and tectonic setting. *Sedimentary Geology*, 341: 289~303.
- Mou Chuanlong, Ge Xiangying, Zhou Kenken, Wang Xiuping. 2015&. Lithofacies palaeogeography in Late Ordovician Wufeng age in southwestern Sichuan. *Geology in China*, 42(1): 192~198.
- Mou Chuanlong, Wang Xiuping, Wang Qiuyi, Zhou Kenken, Liang Wei,

- Ge Xiangying, Chen Xiaowei. 2016&. Relationship between sedimentary facies and shale gas geological conditions of the Lower Silurian Longmaxi Formation in southern Sichuan Basin and its adjacent areas. *Journal of Palaeogeography*, 18(3): 457~472.
- Mou Chuanlong, Ge Xiangying, Yu Qian, Men Xin, Liu Wei, He Jianglin, Liang Wei. 2019&. Palaeoclimatology and provenance of black shales from Wufeng – Longmaxi Formations in southwestern Sichuan Province: From geochemical records of Well Xindi – 2. *Journal of Palaeogeography*, 21(5): 835~846.
- Nie Haikuan, Jin Zhijun, Bian Rui Kang, Du Wei. 2016&. The source–cap hydrocarbon – controlling enrichment of shale gas in Upper Ordovician Wufeng formation–Lower Silurian Longmaxi formation of Sichuan basin and its periphery. *Acta Petrolei Sinica*, 37(5): 557~571.
- Nie Haikuan, Jin Zhijun, Ma Xin, Liu Zhongbao, Lin Tuo, Yang Zhenheng. 2017&. Graptolites zone and sedimentary characteristics of Upper Ordovician Wufeng formation – Lower Silurian Longmaxi formation in Sichuan basin and its adjacent areas. *Acta Petrolei Sinica*, 38(2): 160~174.
- Nesbitt H, Young G. 1984. Prediction of some weathering trends of plutonic and volcanic rocks based on thermodynamic and kinetic considerations. *Geochimica et Cosmochimica Acta*, 48(7): 1523~1534.
- Nesbitt H W, Young G M. 1989. Formation and Diagenesis of Weathering Profiles. *The Journal of Geology*, 97(2): 129~147.
- Nesbitt H M, Young G M. 1982. Early Proterozoic climates and plate motions inferred from major element chemistry of lutites. *Nature*, 299(21): 715~717.
- Pu Boling, Dong Dazhong, Wang Fengqin, Wang Yuman, Huang Jinliang. 2020&. The effect of sedimentary facies on Longmaxi shale gas in southern Sichuan Basin. *Geology in China*, 47(1): 111~120.
- Ren Junping, Zuo Libo, Xu Kangkang, Wang Jie, Liu Xiaoyang, He Shengfei, Liu Yu, He Fuqing. 2016. Geodynamic evolution and mineral resources present research in Bangweulu block, Northern Zambia. *Geological Review*, 62(4): 979~996.
- Roser B P, Korsch R J. 1986. Determination of tectonic setting of sandstone–mudstone suites using content and ratio. *The Journal of Geology*, 94: 635~650.
- Roser B P, Korsch R J. 1999. Geochemical characterization, evolution and source of a Mesozoic accretionary wedge: the Torlesse terrane, New Zealand. *Geological Magazine*, 136: 493~503.
- Rudnick R L, Gao S, Ling W L, Liu Y S, McDonough W F. 2004. Petrology and geochemistry of spinel peridotite xenoliths from Hannuoba and Qixia, North China craton. *Lithos*, 77(1~4): 609~637.
- Sensarma S, Rajamani V, Tripathi J K. 2008. Petrography and geochemical characteristics of the sediments of the small River Hemavati, Southern India: Implications for provenance and weathering processes. *Sedimentary Geology*, 205(3): 111~125.
- Shields G, Stille P. 2001. Diagenetic constraints on the use of cerium anomalies as palaeoseawater redox proxies: an isotopic and REE study of Cambrian phosphorites. *Chemical Geology*, 175(1~2): 29~48.
- Tawfik H A, Ghandour I M, Wataru M, Armstrong-Altrin J S, Abdel-Hameed A – M T. 2015. Petrography and geochemistry of the siliciclastic Araba Formation (Cambrian), east Sinai, Egypt: implications for provenance, tectonic setting and source weathering. *Geological Magazine*, 154(1): 1~23.
- Taylor S R, McLennan S M. 1985. The continental crust: its composition and evolution. Blackwell; Oxford.
- Tian Yang, Zhao Xiaoming, Wang Lingzhan, Tu Bing, Xie Guogang, Zeng Bofu. 2015&. Geochemistry of clastic rocks from the Triassic Xujiahe Formation, Lichuan area, southwestern Hubei: Implications for weathering, provenance and tectonic setting. *Acta Petrologica Sinica*, 31(1): 261~272.
- Tribouillard N, Algeo T J, Baudin F, Riboulleau A. 2012. Analysis of marine environmental conditions based on molybdenum – uranium covariation—Applications to Mesozoic paleoceanography. *Chemical Geology*, 324: 46~58.
- Van de Kamp P C, Leake B E. 1985. Petrography and geochemistry of feldspathic and mafic sediments of the northeastern Pacific margin. *Earth and Environmental Science Transactions of the Royal Society of Edinburgh*, 16(4): 411~449.
- Verma S P, Armstrong – Altrin J S. 2013. New multi – dimensional diagrams for tectonic discrimination of siliciclastic sediments and their application to Precambrian basins. *Chemical Geology*, 355 (5): 117~133.
- Verma S P, Rivera-Gómez M A, Díaz-González L, Pandarinath K, Amezcua-Valdez A, Rosales-Rivera M, Verma S K, Quiroz-Ruiz A, Armstrong-Altrin J S. 2017. Multidimensional classification of magma types for altered igneous rocks and application to their tectonomagmatic discrimination and igneous provenance of siliciclastic sediments. *Lithos*, 278~281: 321~330.
- Wang Qiyu, Mou Chuanlong, He Juan, Yan Guochuan, Ling Yajun, Sun Xiaoyong. 2018&. Provenance analysis and tectonic setting judgment in Shangan Formation of Middle Triassic in Weixi area. *Earth Science*, 43(8): 2811~2832.
- Wang Yuman, Dong Dazhong, Huang Jinliang, Li Xinjing, Wang Shufang. 2016&. Guanyinqiao member lithofacies of the Upper Ordovician Wufeng Formation around the Sichuan Basin and the significance to shale gas plays, SW China. *Petroleum Exploration and Development*, 43(1): 42~50.
- Wang Yuman, Li Xinjing, Dong Dazhong, Zhang Chenchen, Wang Shufang. 2017&. Main factors controlling the sedimentation of high – quality shale in Wufeng – Longmaxi Fm, Upper Yangtze region. *Natural Gas Industry*, 37(4): 9~20.
- Wang Zhongwei, Wang Jian, Fu Xiugen, Zhan Wangzhong, Zeng Shengqiang. 2018. Geochemistry of the Upper Triassic black mudstones in the Qiangtang Basin, Tibet: Implications for paleoenvironment, provenance, and tectonic setting. *Journal of Asian Earth Sciences*, 160: 118~135.
- Wang Zhongwei, Wang Jian, Fu Xiugen, Zhan Wangzhong, Yu Fei, Feng Xinglei, Song Chunyan, Chen Wenbin, Zeng Shengqiang. 2017. Organic material accumulation of Carnian mudstones in the North Qiangtang Depression, eastern Tethys: Controlled by the paleoclimate, paleoenvironment, and provenance. *Marine and Petroleum Geology*, 88: 440~457.
- Wu Anbin, Zhang Jingkun, Wang Jingling, Luo Jiagu, Luo Qun, Jiang Zhenxue. 2020. Genesis, diagenetic model and geological significance of calcite veins in organic rich shale: a case study of the Longmaxi Formation, southern Sichuan basin, China. *Geological Review*, 66(1): 88~99.
- Wu Lanyu, Hu Dongfeng, Lu Yongchao, Liu Ruobing, Liu Xiaofeng. 2016&. Advantageous shale lithofacies of Wufeng Formation – Longmaxi Formation in Fuling gas field of Sichuan Basin, SW

- China. Petroleum Exploration and Development, 43(2): 189~197.
- Yan Detian, Wang Qingchen, Chen Daizhao, Wang Jianguo, Wang Zhuozhuo. 2008&. Sedimentary Environment and Development Controls of the Hydrocarbon Sources Beds: the Upper Ordovician Wufeng Formation and the Lower Silurian Longmaxi Formation in the Yangtze Area. Acta Geologica Sinica, 82(3): 321~327.
- Yu Qian, MouChuanlong, Zhang Haiquan, Tan Qinyin, Xu Xiaosong, Yan Jianfei. 2011&. Sedimentary evolution and reservoir distribution of northern Upper Yangtze plate in Sinian – Early Paleozoic. Acta Petrologica Sinica, 27(3): 672~680.
- Yuan Tao, Wei Xiangfeng, Zhang Hanrong, Li Chunyan, Wei Fubin, Lu Longfei, Wang Qiang. 2020&. Shale petrofacies division of Wufeng–Longmaxi formations in Sichuan basin and its periphery. Petroleum Geology and Experiment, 42(3): 371~381.
- Zhang Jianjun, Mou Chuanlong, Zhou Kenken, Feng Lixai, Wu Hao, Chen Xiaowei. 2017&. Geochemical characteristic of sandstones from the Mangbang formation in the Husa basin, western Yunnan, and its constraints on provenances and tectonic setting. Acta Geologica Sinica, 91(5): 1083~1096.
- Zhang Jinliang, Zhang Xin. 2007&. Element geochemistry of sandstones in the Silurian of central Tarim basin and the significance in provenance discrimination. Acta Petrologica Sinica, 23(11): 2990~3002.
- Zhang Qian, Wang Jian, Yu Qian, Wang Xiaofei, Zhao Ankun, Lei Zihui. 2016&. Geochemical Features and Paleoenvironment of Shales in Longmaxi Formation of Complicated Structure Area, Southwestern Sichuan Basin. Xing Jiang Petroleum Geology, 38(4): 399~406.
- Zhang Qian, Yu Qian, Wang Jian, Xiao Yuanfu, Cheng Jinxiang, Zhao Ankun, Zhang Bin. 2018a&. Application of ICP–MS to study the Rare Earth Element characteristics and sedimentary environment of black shale in the Longmaxi formation in the Southwestern Sichuan Basin. Rock and Mineral Analysis, 37(2): 217~224.
- Zhang Qian, Wang Jian, Yu Qian, Xiao Yuanfu, Zhang Bin, Wang Xiaofei, Zhao Ankun. 2018b&. The Silicon Source and Sedimentary Environment of the Lower Silurian Longmaxi Formation in Yanyuan Basin, Western Edge of the Yangtze Platform. Geological Review, 64(3): 610~622.
- Zhao Zhenhua. 1978&. Geochemical characteristics of rare earth elements and their applications in the study of the genesis of rocks and ore deposits. Earth and Environment, 33(9): 3~13.
- Zheng Zhihong, Li Denghua, Bai Senshu, Jia Jun, Zan Xin, Liu Zhuoya, Gao Xuan. 2017&. Resource potentials of natural gas in Sichuan Basin. China Petroleum Exploration, 22(3): 12~20.
- Zhou Lian, Algeo T J, Shen Jun, Hu ZhiFang, Gong Hongmei, Xie Shucheng, Huang Junhua, Gao Shan. 2015. Changes in marine productivity and redox conditions during the Late Ordovician Hirnantian glaciation. Palaeogeography, Palaeoclimatology, Palaeoecology, 420: 223~234.
- Zhou Yuanyuan, Qiu Nansheng, Tenger, Wang Jie, Cao Taotao, Luo Houyong. 2016&. Geochemical characteristics and the geological significance of oil shales from the Youganwo Formation, Maoming basin, China. Bulletin of Mineralogy Petrology and Geochemistry, 35(6): 1270~1279.
- Zhou Kenken, Xu Xiaosong. 2016&. Evolution of paleo-uplifts in the western upper Yangtze craton and its reflection on Yunan orogeny. Geological Review, 62(5): 1125~1133.
- Zhong Yong, Li Yalin, Zhang Xiaobin, Liu Shugen, Wu Furong, Liu Dingjin, Deng Xiaojiang, Chen Sheng, Yang Fei, Li Xiaojuan, Jiang Bo. 2014&. Evolution characteristics of central Sichuan palaeouplift and its relationship with Early Cambrian Mianyang–Changning intracratonic sag. Journal of Chengdu University of Technology ( Science & Technology Edition), 45(6): 703~712.

## Geochemistry of the Longmaxi Formation mudstones of the southwest Sichuan Basin: Implications for provenance and source weathering

ZHANG Qian<sup>1, 2, 3)</sup>, XIAO Yuanfu<sup>1)</sup>, WANG Xiaofei<sup>2, 3)</sup>, YU Qian<sup>2, 3)</sup>, WANG Jian<sup>4)</sup>, ZHAO Ankun<sup>1, 2, 3)</sup>, MENG Yupeng<sup>2, 3)</sup>, ZHOU Yixin<sup>2, 3)</sup>

1) School of Earth Sciences, Chengdu University of Technology, Chengdu, 610059;

2) Chengdu Geological Survey Center, China Geological Survey, Chengdu, 610081;

3) Key Laboratory of Sedimentary Basin and Oil & Gas Resources, Ministry of Natural Resources, Chengdu, 610081;

4) School of Geoscience and Technology, Southwest Petroleum University, Chengdu, 610500

**Objectives:** This article mainly discusses the depositional environment, provenance characteristics and sedimentary tectonic background of the Longmaxi Fm mudstone in the Yingjing area, southwestern margin of the Sichuan Basin. The correspondence relationship between mudstone and source rocks was initially established to support the related basic geological research of regional shale gas exploration and development.

**Methods:** The detailed geological survey and systematic research on petrology, mineralogy, element geochemistry were used to study the Longmaxi Formation.

**Results:** The content of sandstone and calcareous of the Longmaxi Fm is relatively high, This indicates a shallow water deposition environment. The characteristics of REE and A-CN-K diagram show the mudstone of the Longmaxi Fm is less affected by diagenesis and metasomatism. The high content of  $K_2O$ , Rb and  $Al_2O_3/TiO_2$  and

the negative  $\delta\text{Eu}_N$  indicate that the source rocks are feldspathic igneous rocks and granite. The  $ICV > 1$ ,  $CIA = 66$ ,  $\text{Th}/\text{U}$  is similar to the UCC value,  $\text{Rb}/\text{Sr}$  is significantly lower than PAAS, indicating that its source is the rapid deposition product of the first cycle of the near source.  $\text{La}/\text{Yb}$ , LREE/HREE and  $\text{Sc}/\text{Cr}$  were similar to those of passive continental margin.

**Conclusions:** Affected by tectonic uplift, the entire Longmaxi Fm in the study area was a shallow-water continental shelf sediment, and the sedimentary background was mainly the passive continental marginal environment. The source rocks was mainly provided by the early Neoproterozoic platform cover of Kangtien old land on the west side. The paleoclimate of the provenance was cold and dry, and experienced low-level chemical weathering.

**Keywords:** Longmaxi Formation; element geochemistry; provenance; tectonic background; Sichuan Basin; Yingjing area; geological survey engineering

**Acknowledgements:** Supported by the National Science and Technology Major special Project "Shale Gas Exploration and Evaluation Technology Test and Application Promotion" (No. 2016ZX05034-004)

**First author:** ZHANG Qian, female, born in 1983, engineer, mainly engaged in shale gas and conventional oil and gas geological survey and evaluation; Email: 76517507 @ qq. com

Manuscript received on: 2019-08-14; Accepted on: 2020-07-27; Edited by: LIU Zhiqiang

**Doi:** 10. 16509/j. georeview. 2020. 05. 022